

DTIC FILE COPY

4

GL-TR-89-0096

ENVIRONMENTAL RESEARCH PAPERS, NO. 1027

AD-A220 004

An Analytic/Empirical Model of the
Middle and Low Latitude Ionosphere

J.M. Forbes
D.N. Anderson
M. Codrescu
P.P. Batista



31 March 1989



Approved for public release; distribution unlimited.



DTIC
ELECTE
APR 02 1990
S E D

IONOSPHERIC PHYSICS DIVISION

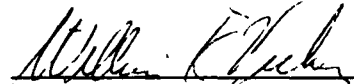
PROJECT 2310

GEOPHYSICS LABORATORY

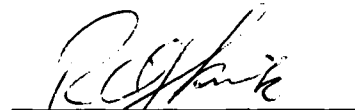
HANSCOM AFB, MA 01731-5000

90 04 02 113

"This technical report has been reviewed and is approved for publication"


WILLIAM K. VICKERY
Acting Branch Chief

FOR THE COMMANDER


ROBERT A. SKRIVANEK
Division Director

This report has been reviewed by the ESD Public Affairs Office (PA) and is releasable to the National Technical Information Service (NTIS).

Qualified requestors may obtain additional copies from Defense Technical Information Center.

If your address has changed, or if you wish to be removed from the mailing list, or if the addressee is no longer employed by your organization, please notify AFGL/DAA, Hanscom AFB, MA 01731. This will assist us in maintaining current mailing list.

Do not return copies of this report unless contractual obligations or notice on a specific document requires that it be returned.

UNCLASSIFIED

SECURITY CLASSIFICATION OF THIS PAGE

REPORT DOCUMENTATION PAGE

Form Approved
OMB No. 0704-0188

1a. REPORT SECURITY CLASSIFICATION Unclassified			1b. RESTRICTIVE MARKINGS		
2a. SECURITY CLASSIFICATION AUTHORITY N/A			3. DISTRIBUTION / AVAILABILITY OF REPORT Approved for public release; distribution unlimited.		
2b. DECLASSIFICATION / DOWNGRADING SCHEDULE N/A					
4. PERFORMING ORGANIZATION REPORT NUMBER(S) GL-TR-89-0096 ERP, No. 1027			5. MONITORING ORGANIZATION REPORT NUMBER(S)		
6a. NAME OF PERFORMING ORGANIZATION Geophysics Laboratory		6b. OFFICE SYMBOL (If applicable) LIS		7a. NAME OF MONITORING ORGANIZATION	
6c. ADDRESS (City, State, and ZIP Code) Hanscom AFB Massachusetts 01731-5000			7b. ADDRESS (City, State, and ZIP Code)		
8a. NAME OF FUNDING / SPONSORING ORGANIZATION		8b. OFFICE SYMBOL (If applicable)		9. PROCUREMENT INSTRUMENT IDENTIFICATION NUMBER	
8c. ADDRESS (City, State, and ZIP Code)			10. SOURCE OF FUNDING NUMBERS		
			PROGRAM ELEMENT NO. 61102F	PROJECT NO. 2310	TASK NO. G9
			WORK UNIT ACCESSION NO. 03		
11. TITLE (Include Security Classification) An Analytic/Empirical Model of the Middle and Low Latitude Ionosphere					
12. PERSONAL AUTHOR(S) Forbes, J.M.*, Anderson, D.N., Codrescu, M.*, and Batista, P.P.†					
13a. TYPE OF REPORT Scientific Interim		13b. TIME COVERED FROM _____ TO _____		14. DATE OF REPORT (Year, Month, Day) 1989 March 31	
15. PAGE COUNT 54					
16. SUPPLEMENTARY NOTATION *Boston University, Ctr. for Space Physics & Dept. of Electrical, Computer, & Systems Engineering, Boston, MA 02215; **NCAR/HAO, Boulder, CO 80307; †INPE, Sao Paulo, Brazil					
17. COSATI CODES			18. SUBJECT TERMS (Continue on reverse if necessary and identify by block number)		
FIELD	GROUP	SUB-GROUP	Electron densities, Ionospheric model, Ionosphere, neutral atmosphere coupling, <i>61102F</i>		
19. ABSTRACT (Continue on reverse if necessary and identify by block number) An improved analytic/empirical model of F-layer plasma density is developed by modifying the Chiu (1975) model so as to (a) better approximate middle latitude F-layer peak heights (hmF2's) as derived from ionosonde data, and (b) better model features such as the post-sunset rise in the F-layer peak height, and the "equatorial anomaly" maxima in plasma density near $\pm 15^\circ$ geomagnetic latitude. The latter is accomplished by applying analytic low-latitude correction as derived from differences between the Chiu model and the SLIM model of Anderson et al. Results of a numerical model are also presented that demonstrate the importance of these low-latitude plasma structures to the neutral dynamics of the thermosphere.					
20. DISTRIBUTION/AVAILABILITY OF ABSTRACT <input checked="" type="checkbox"/> UNCLASSIFIED/UNLIMITED <input type="checkbox"/> SAME AS RPT. <input type="checkbox"/> DTIC USERS			21. ABSTRACT SECURITY CLASSIFICATION Unclassified		
22a. NAME OF RESPONSIBLE INDIVIDUAL David N. Anderson			22b. TELEPHONE (Include Area Code) 617-377-3982		22c. OFFICE SYMBOL AFGL/LIS

DD FORM 1473, JUN 86

Previous editions are obsolete.

SECURITY CLASSIFICATION OF THIS PAGE

UNCLASSIFIED

Preface

M. Codrescu acknowledges support under Grant AFOSR-85-0048 from the U.S. Air Force Office of Scientific Research to Boston University for development of the neutral dynamical model described herein.

Accession For	
NTIS GRA&I	<input checked="" type="checkbox"/>
DTIC TAB	<input type="checkbox"/>
Unannounced	<input type="checkbox"/>
Justification	
By	
Distribution/	
Availability Code	
Dist	Avail and/or Special
A-1	



Contents

1. INTRODUCTION	1
2. THE APPROACH	2
3. ANALYTIC FORMULATION	3
3.1 Middle Latitude Correction	3
3.2 Low Latitude Correction	4
4. RESULTS	7
5. NEUTRAL DYNAMICS IMPLICATIONS	10
REFERENCES	15
APPENDIX A: LATITUDE VARIATION IN THE DIURNAL, SEMIDIURNAL AND TERDIURNAL PHASE AND AMPLITUDE COMPONENTS OF HMF2 AND FOF2 IN THREE LONGITUDE SECTORS DURING SEPTEMBER 1984.	17
APPENDIX B: LATITUDE VARIATION IN THE DIURNAL, SEMIDIURNAL AND TERDIURNAL PHASE AND AMPLITUDE COMPONENTS OF HMF2 AND FOF2 IN THREE LONGITUDE SECTORS DURING MARCH 1979.	33

Illustrations

1. Monthly Mean hmF2s at Wakkanai (45.4°N, 141.7°E Geographic; 35.5°N, 107.3°E Geomagnetic) for September, 1984, and March, 1979, are Compared with Chiu and FAIM Values	5
2. Monthly Mean hmF2s at Dakar (14.8°N, 342.6°E Geographic; 21.4°N, 56.0°E Geomagnetic) During September, 1984, Compared with Chiu and FAIM Values	6
3. Comparison of hmF2 and foF2 Values as a Function of Dip Latitude at 1400 LT Given by SLIM, Chiu, and FAIM for Solar Cycle Maximum, Equinoctial Conditions	8
4. Same as Figure 3 Except at 2000 LT	9
5. (a) Comparison Between SLIM, Chiu, and FAIM Electron Density Profiles at the Magnetic Equator at 2000 LT. (b) Same as (a), Except at 16°S Dip Latitude	11
6. (a) Calculated Eastward Neutral Winds at the Equator for Solar Maximum Conditions Using the Chiu Plasma Density Model. (b) Same as (a), Except for FAIM Plasma Density Model. (c) (b) Minus (a). (d) Same as (c), Except for Solar Minimum	13
A1. Diurnal and Monthly Mean hmF2s from Ionosonde Stations in the Three Longitude Sectors. Sector 1: Europe, Africa, W. Asia; Sector 2: Asia, Pacific; Sector 3: America, Greenland, During September, 1984, and Compared to the SLIM and FAIM Models	19
A2. Same as A1, Except for Diurnal Amplitude	20
A3. Same as A1, Except for Semidiurnal Amplitude	21
A4. Same as A1, Except for Terdiurnal Amplitude	22
A5. Same as A1, Except for Diurnal Phase	23
A6. Same as A1, Except for Semidiurnal Phase	24
A7. Same as A1, Except for Terdiurnal Phase	25
A8. Same as A1, Except for foF2	26

Illustrations

A9. Same as A2, Except for foF2	27
A10. Same as A3, Except for foF2	28
A11. Same as A4, Except for foF2	29
A12. Same as A5, Except for foF2	30
A13. Same as A6, Except for foF2	31
A14. Same as A7, Except for foF2	32
B1. Diurnal and Monthly Mean hmF2s from Ionosonde Stations in the Three Longitude Sectors, Sector 1: Europe, Africa, W. Asia; Sector 2: Asia, Pacific; Sector 3: America, Greenland, During March, 1979, and Compared to the SLIM and FAIM Models	35
B2. Same as B1, Except for Diurnal Amplitude	36
B3. Same as B1, Except for Semidiurnal Amplitude	37
B4. Same as B1, Except for Terdiurnal Amplitude	38
B5. Same as B1, Except for Diurnal Phase	39
B6. Same as B1, Except for Semidiurnal Phase	40
B7. Same as B1, Except for Terdiurnal Phase	41
B8. Same as B1, Except for foF2	42
B9. Same as B2, Except for foF2	43
B10. Same as B3, Except for foF2	44
B11. Same as B4, Except for foF2	45
B12. Same as B5, Except for foF2	46
B13. Same as B6, Except for foF2	47
B14. Same as B7, Except for foF2	48

Tables

1. Ionosonde Stations Utilized for Data Depicted in Figures A1 - A14 (September 1984)	18
2. Ionosonde Stations Utilized for Data Depicted in Figures B1 - B14 (March 1979)	34

An Analytic/Empirical Model of the Middle and Low Latitude Ionosphere

1. INTRODUCTION

Recently, a Semi-empirical Low-latitude Ionospheric Model (SLIM) was developed¹ that provides F-region electron and ion (O^+) density profiles from 180 km to 1000 km every 2° latitude ($24^\circ N$ to $24^\circ S$) and every one-half hour local time over the 24-hour day. The reason for producing this model was to generate, in a computationally efficient manner, electron density profiles at low latitudes that were more realistic than those of the widely used empirical models of Chiu² or Bent.³ SLIM consists of functions and coefficients that reproduce 9 sets of theoretically-calculated low-latitude electron density profiles corresponding to the three seasons: equinox, June solstice, and December solstice for three levels of solar activity: solar minimum ($F_{10.7} = 70$), moderate solar activity ($F_{10.7} = 125$), and solar maximum ($F_{10.7} = 185$). A separate set of six coefficients exist for each 2° interval in latitude and each one-half hour interval in local time. The profiles are determined by the six parameters, $nmF2$, $hmF2$, H_{UP} , H_{LO} , C_{UP} , and C_{LO} and the modified Chapman expression:

$$N_e(Z) = nmF2 \times \exp[C(1 - Z - \exp(-Z))] \quad (1)$$

(Received for Publication 30 March 1989)

1. Anderson, D.N., Mendillo, M., and Herniter, B. (1987a) A semi-empirical, low-latitude ionospheric model, *Radio Sci.* **22**:292-306.
2. Chiu, Y.T. (1975) An improved phenomenological model of ionospheric density, *J. Atmos. Terr.* **37**:1563-1570.
3. Llewellyn, S.K. and Bent, R.B. (1973) *Documentation and Description of the Bent Ionospheric Model*, AFCRL-TR-73-0657, AD 772733, Air Force Cambridge Research Laboratories, Bedford, MA.

where nmF2 is the peak plasma density, hmF2 is the altitude where $N_e(Z) = \text{nmF2}$, $Z = \frac{h - \text{hmF2}}{H}$, and the subscripts _{UP} and _{LO} refer, respectively, to those regions above and below hmF2. While electron density profiles are easily generated from the various sets of coefficients given in tabular form, a more convenient approach would be to specify the coefficients as analytic functions of local time and latitude, as in the Chiu² empirical model. Furthermore, because the Chiu ionospheric model has been so extensively used to specify the low- and middle-latitude ionospheric region, it was decided to recast the coefficients in an analytic form so that present users of the Chiu model would have access to the new, improved formulation without having to modify any of the input and output parameters.

This report describes briefly the technique used to generate the analytic functions that would reproduce the SLIM profiles, and then compares this Fully Analytic Ionospheric Model (hereafter referred to as FAIM) with SLIM and the Chiu empirical ionospheric model to illustrate the similarities and differences, respectively. We then demonstrate the importance of using a realistic low-latitude ionospheric model when calculating the local time variation in zonal winds from the dynamical neutral wind equations.

2. THE APPROACH

The empirical Chiu ionospheric model is based on middle- and low-latitude observations of the E, F1, and F2 regions of the ionosphere which cover seasonal as well as solar cycle variations. The model assumes that the F2-region plasma density can be expressed by the Chapman profile expression

$$N_e(Z) = \text{nmF2} \times \exp[1 - Z - \exp(-Z)], \quad (2)$$

where the variables are the same as in Eq. (1), and the coefficient C is taken to be unity. As in SLIM, the Chiu formulation utilizes two expressions for Z, one for the bottomside of the F-layer and one for the topside, given respectively by

$$Z_{\text{LO}} = \frac{h - \text{hmF2}}{H_{\text{LO}}} \quad (3)$$

$$Z_{\text{UP}} = \frac{h - \text{hmF2}}{H_{\text{UP}}} \quad (4)$$

In all, four coefficients are needed to completely specify the F2-layer in the Chiu model: nmF2, hmF2, H_{UP} and H_{LO} . Similar formulations are utilized for the F1- and E-layers, and the total plasma density as a function of altitude is obtained by summing these three contributions. Analytic functions are used throughout to express the coefficients as a function of geographic and geomagnetic coordinates, sunspot number, local time, and day of year.

The Chiu model is widely known to be deficient in its specification of hmF2 at middle and low latitudes, and its representation of the equatorial anomaly. In our approach, we have first applied a correction to the Chiu hmF2s at middle and low latitudes based on ionosonde data. Then, we have added analytic corrections for foF2 and hmF2 and modified H_{UP} and H_{LO} in the Chiu model between $\pm 24^\circ$ dip latitude, such that the ionization profiles best fit those of the SLIM model. In FAIM we no longer use the modified Chapman function (1) which contains the C_{UP} and C_{LO} coefficients. The above procedure and the equations involved are detailed below.

3. ANALYTIC FORMULATION

3.1 Middle Latitude Correction

The middle latitude correction to the hmF2 specification of the Chiu model is based on examination of a rather limited set of monthly mean ionosonde measurements (about 40 stations) covering only September 1984 (a solar minimum period with $F_{10.7} \approx 80$) and March 1979 (a solar maximum period with $F_{10.7} \approx 180$). These months were chosen because they include the Equinox Transition Study (ETS) campaign and the CDAW-6 interval, and hence the data were readily available to us. Our main interest here is to provide a significantly improved and easy to use analytic/empirical model of the low-latitude ionosphere. However, when we realized how poor the F-layer peak heights (hmF2s) in the Chiu² model really were, we decided to apply a first-order correction to these, prior to deriving the low-latitude correction based on SLIM. Certainly, these middle-latitude corrections ought to be scrutinized and improved upon using data with broader coverage in season and solar cycle, but this effort is viewed out of the scope of the present study. We did, however, find the Chiu values for foF2 to match the ionosonde data reasonably well, and did not attempt any corresponding corrections to this ionospheric parameter.

The original expression for hmF2 in Chiu² is:

$$\text{hmF2} = 240 + 75\rho + 83\rho\zeta\cos\lambda_m + 30\cos(\phi - 4.5|\lambda_m| - \pi) + 10\cos\lambda_m\cos\frac{\pi}{3}(t - 4.5) \quad (5)$$

where

- t = annual time (days of year) in units of months as measured from 15 December of the previous year
- ρ = $R/100$
- R = the monthly smooth Zurich sunspot number
- λ_m = geomagnetic latitude (rad)
- ζ = $\sin\delta\sin\lambda_m$ where δ = solar angle (rad)
- ϕ = local time angle (rad) measured from local midnight.

Note that the local time variation consists only of a diurnal (24-hour harmonic) that is independent of season and solar cycle. Our correction concerns the second (solar cycle) and fourth (local time) terms in the above equation. The former is replaced by

$$100\sqrt{\rho} - 10. \quad (6)$$

The local time term is replaced by

$$(56 - 12\sqrt{\rho})\cos(\phi + \lambda_\alpha) + (9 + 12\sqrt{\rho})\cos(2\phi - \frac{\pi}{4}) + 12\cos(3\phi - \frac{3\pi}{4}) \quad (7)$$

where

$$\lambda_\alpha = -2\pi + \frac{3\pi}{4} e^{-\left(\frac{\lambda_m}{.349}\right)^2}. \quad (8)$$

Thus, we have modified the mean value and solar cycle dependence of the diurnal average component of hmF2, have modified the diurnal (24-hour) component to reflect a solar cycle dependence, and in addition, have added semidiurnal (12-hour) and terdiurnal (8-hour) components to

the expression for hmF2. These dependences were derived by examining the local time Fourier components of hmF2 and foF2 from global ionosonde data during September, 1984, and March, 1979, as mentioned previously. These data are illustrated in the Appendixes of this report in Figures A1-A14 and B1 - B14, respectively, and are compared there to values from the expressions above, as well as to the low-latitude corrections derived from the SLIM model, to be described below.

Comparisons between the local time variations of hmF2 as observed at Wakkanai (45.4° latitude), Dakar (14.8° latitude), and Moscow (55.5° latitude) are illustrated in Figures 1 and 2. These are typical of comparisons with most other stations. In Figure 1, the solar cycle dependence of hmF2 at Wakkanai is seen to be well modelled by the above equations, and represents a considerably better fit to the data than Chiu.² Figure 2 illustrates the latitude dependence of the local time variation of hmF2 during solar minimum conditions. Again, the newly defined hmF2 representation reproduces the ionosonde data extremely well, reflecting an impressive improvement over the Chiu formulation.

3.2 Low Latitude Correction

In developing the low-latitude portion of FAIM, we derive new analytic formulations for the parameters foF2, hmF2, H_{UP} , and H_{LO} in the Chiu model based on least-squares fits to the SLIM profiles. The local time variation at a given dip latitude (λ_m) is expressed as a series of sines and cosines with amplitudes a_n and b_n with the series going from $n = 0$ to $n = 6$:

$$f(\lambda, \phi) = \sum_{n=0}^6 (a_n(\lambda) \sin(n\phi) + b_n(\lambda) \cos(n\phi)) \quad (9)$$

where ϕ is local time from midnight in radians. A separate function $f_s(\lambda, \phi)$ is found for each of the four defining parameters, $s = 1$ to 4.

In reality, for foF2 and hmF2 values, we used the expression above to fit the difference between the Chiu and SLIM values so that in the new analytic model, we simply calculate the Chiu values and then add to these the analytically-formulated difference values to provide the final foF2 and hmF2 quantities specified by FAIM. The procedure for obtaining the topside and bottomside F-region scale heights, H_{UP} and H_{LO} is handled somewhat differently. Here, a separate topside and bottomside scale height was found which would reproduce each SLIM profile density to within 0.5 MHz assuming the expression for $N_e(Z)$ given by Eq. (2). These scale heights are different from those specified in the paper by Anderson et al.¹ because the values for C_{UP} and C_{LO} are now assumed to be unity. Once values of H_{UP} and H_{LO} were obtained by this method, the analytic functions given by Eq. (9) were derived.

The next task was to find appropriate functions and coefficients that would reproduce the separate sets of a_n 's and b_n 's as a function of dip latitude (λ_m). The modified harmonic oscillator function $H_k(\psi)e^{-\psi^2}$ where H_k is the Hermite Polynomial of order k and $\psi = \frac{\lambda_m}{244}$ (λ_m in radians) was found to be ideally suited for this purpose:

$$a_n(\lambda_m), b_n(\lambda_m) = \sum_{k=0}^4 C_k H_k(\psi) e^{-\psi^2}. \quad (10)$$

The FAIM FORTRAN code is basically the Chiu² code with the corrections outlined above incorporated.

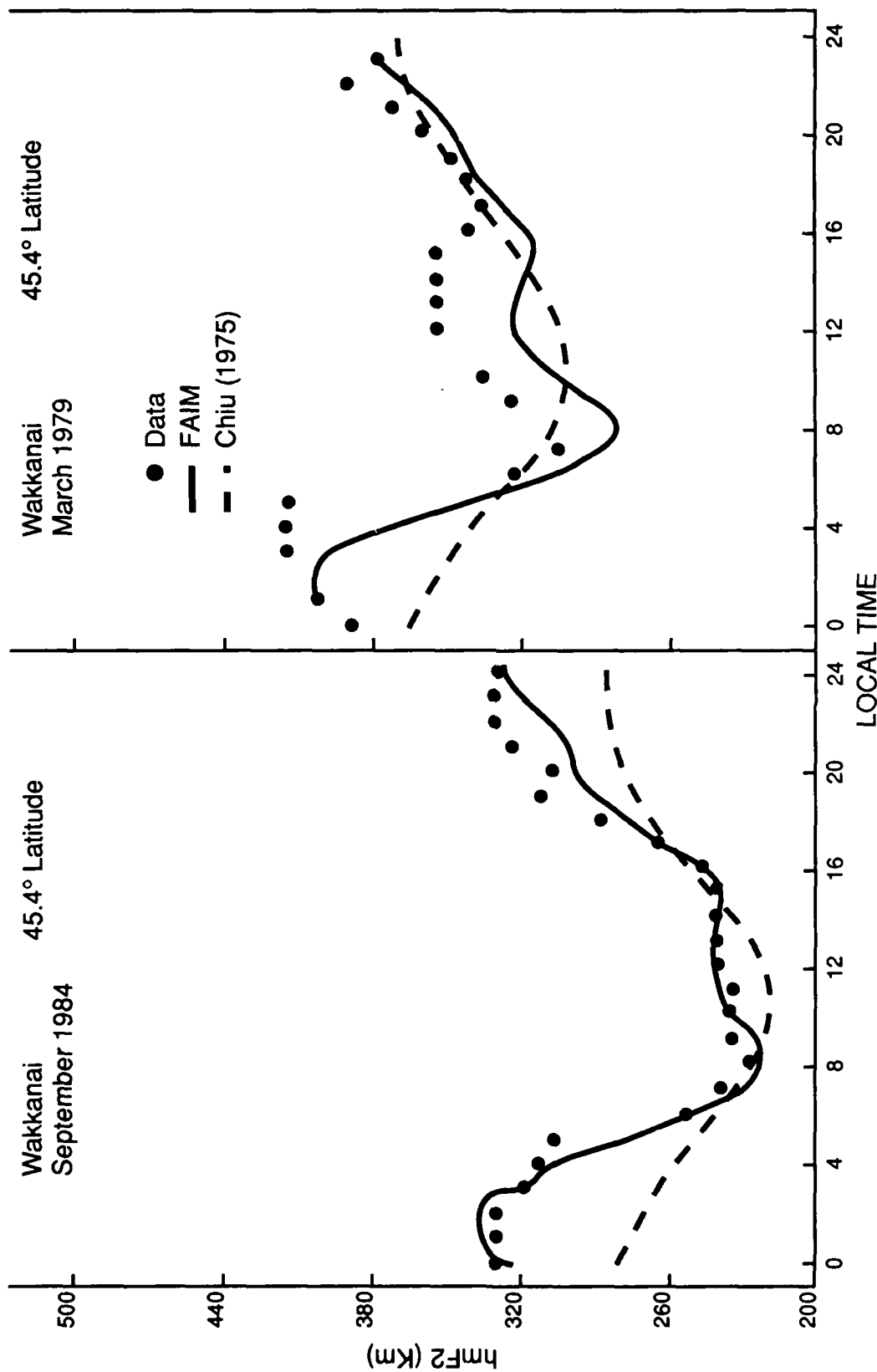


Figure 1. Monthly Mean hmF2s at Wakkanai (45.4°N, 141.7°E Geographic; 35.5°N, 107.3°E Geomagnetic) for September, 1984, and March, 1979, are Compared with Chiu and FAIM Values. The hmF2s are computed empirically from foF2, MU(3000), and foE using the formulas of Bradley and Dudeney⁴ (1973).

4. Bradley, P.A. and Dudeney, J.R. (1973) A simple model of the vertical distribution of electron concentration in the ionosphere, *J. Atmos. Terr. Phys.* **35**:2131.

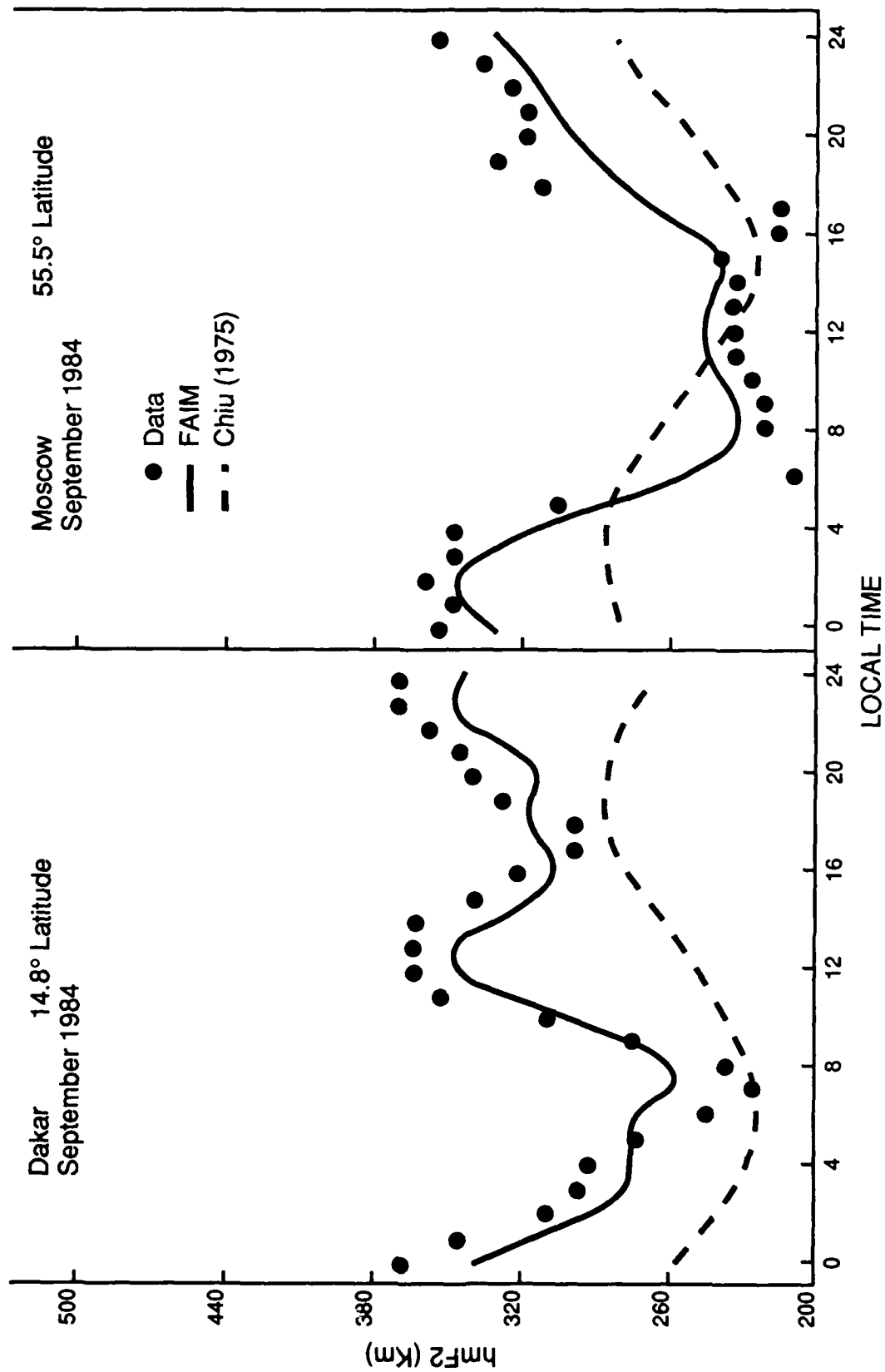


Figure 2. Monthly Mean hmF_2 s at Dakar (14.8°N, 342.6°E Geographic; 21.4°N, 56.0°E Geomagnetic) and Moscow (55.5°N, 39.3°E Geographic; 50.4°N, 123°E Geomagnetic) Compared with Chiu and FAIM Values. The hmF_2 values are computed as in Figure 1.

4. RESULTS

As outlined in the paper by Anderson et al¹, nine separate SLIM cases were generated covering three levels of solar activity; low, moderate, and high for each of three seasons; equinox, June solstice, and December solstice. For these nine cases, sets of coefficients to the analytic functions described above were determined that would reproduce the local time and latitude variations in the four parameters foF2, hmF2, H_{UP} , and H_{LO} .

To demonstrate how well FAIM reproduces the SLIM values, we plot in Figure 3 the latitude variation in hmF2 and foF2 at 1400 LT for the solar cycle maximum, equinox case. In this figure, we also compare these models with the empirical Chiu values for hmF2 and foF2. Looking first at the hmF2 comparisons, FAIM smooths out the SLIM values between 12°N and 12°S dip latitude and gives excellent agreement poleward of $\pm 12^\circ$. Actually, the large variation in SLIM hmF2 between $\pm 4^\circ$ and $\pm 10^\circ$ dip latitude is somewhat an artifact of the SLIM least-squares approach so that the smoother variation in FAIM hmF2 values is actually more realistic. The comparison of both SLIM and FAIM with the Chiu model illustrates the magnitude of the improvement at low latitudes. As reported by Rajaram and Rastogi⁵, daytime hmF2 values near the magnetic equator at Kodaikanal, India lie in the range 450 to 500 km, about 100 km greater than the 350 km specified in the Chiu model.

The comparison in foF2 between FAIM and SLIM is excellent. The analytic model slightly overestimates SLIM values near the crests of the equatorial anomaly at $\pm 16^\circ$ to $\pm 20^\circ$ dip latitude and underestimates slightly near the magnetic equator, but these differences are well within the day-to-day fluctuations in equatorial foF2 values. A comparison with the Chiu model shows the crest-to-trough density ratio is greater for the analytic model, which is in good agreement with observed values in the Indian sector during March 1959, a solar cycle maximum equinoctial period.⁵

At 2000 LT, the comparison between SLIM, FAIM, and Chiu are even more impressive as shown in Figure 4. The post-sunset enhancement in upward $E \times B$ drift is a characteristic feature during equinox, solar maximum years⁶ and is responsible for the very high hmF2 values near the magnetic equator.⁷ It is reproduced in both SLIM and FAIM. Such high hmF2 values are also in agreement with measured values at Kodaikanal⁴ and at Jicamarca.¹ The analytic model reproduces the latitude variation in SLIM values very well and both these models give substantially greater hmF2 values than the Chiu model.

An unrealistically low F-layer peak height is provided by the Chiu model and can have significant consequences if it is used in neutral dynamics calculations. In particular, after sunset when the two main horizontal forces on the neutrals are the pressure gradient and ion drag forces, the low hmF2's and, hence, unrealistically large plasma densities are expected to result in significant

5. Rajaram, G. and Rastogi, R.G. (1977) Equatorial electron densities-seasonal and solar cycle changes, *J. Atmos. Terr. Phys.* **39**:1175-1182.

6. Rastogi, R.G. (1966) The equatorial anomaly in the F2 region of the ionosphere, *Inst. Telecomm. Engrs.* **12**:245-256.

7. Woodman, R.F. (1970) Verticle drift velocities and east-west electric fields at the magnetic equator, *J. Geophys. Res.* **75**:6249-6259.

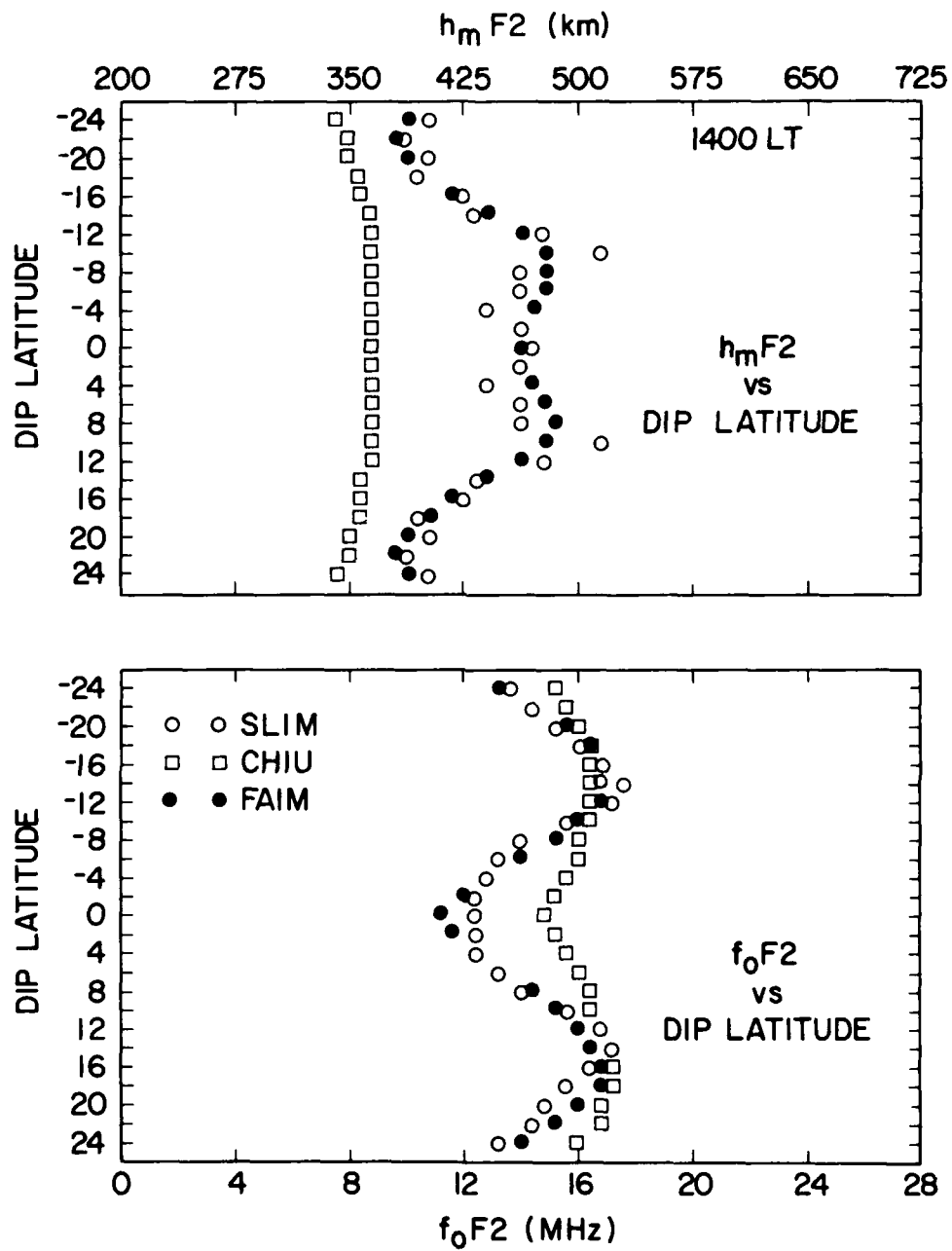


Figure 3. Comparison of $h_m F2$ and $f_o F2$ Values as a Function of Dip Latitude at 1400 LT Given by SLIM, Chiu, and FAIM for Solar Cycle Maximum, Equinoctial Conditions.

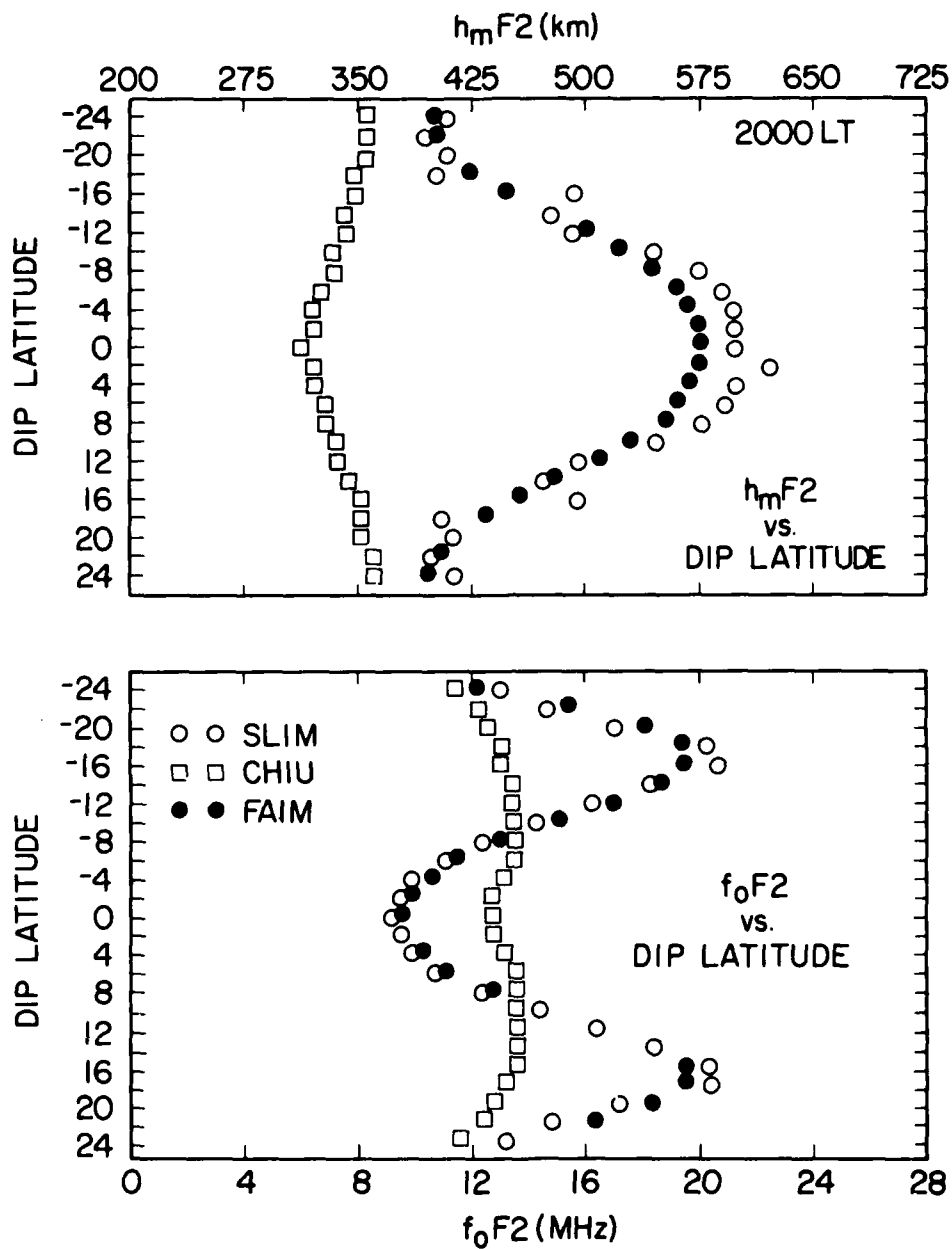


Figure 4. Comparison of $h_m F2$ and $f_o F2$ Values as a Function of Dip Latitude at 2000 LT Given by SLIM, Chiu, and FAIM for Solar Cycle Maximum, Equinoctial Conditions.

underestimates of the zonal wind speed.⁸

The enhancement in the upward $E \times B$ drift velocity at the equator mentioned above is also responsible for maintaining the crests of the anomaly out to $\pm 18^\circ$ dip latitude and increasing the peak-to-trough ratio after sunset. This latitude variation in foF2 at 2000 LT is completely absent in the Chiu model, which essentially displays a constant density value with latitude. The more realistic FAIM and SLIM models with peak densities of 5×10^6 el/cm³ (foF2 ~ 18 MHz) at the crests of the anomaly, provide much greater ion drag forces at these latitudes, which translate to a greater latitude variation in the zonal neutral wind velocities. In addition, this latitude structure in peak densities significantly affects flux tube integrated conductivities after sunset that play an important role in the electrical coupling between the low-latitude ionosphere and neutral atmosphere.⁹

A comparison of profile shapes at the magnetic equator and at 16° S dip latitude is illustrated in Figure 5 for the 2000 LT period. At the magnetic equator, reasonable agreement between FAIM and SLIM is achieved with the topside portion being in better agreement than the bottomside region. Actually, this represents one of the poorest fits of all the comparisons. The degree to which both FAIM and SLIM profiles differ from the Chiu model is graphically illustrated and displays the unrealistically large electron density values in the 350 km region provided in the Chiu model. At 16° S dip latitude, the comparison between FAIM and SLIM is excellent and is more indicative of the general agreement that can be achieved when analytic functions for H_{UP} and H_{LO} are used to calculate profile shapes. Here, FAIM and SLIM foF2 and hmF2 values are significantly greater than Chiu values.

5. NEUTRAL DYNAMICS IMPLICATIONS

As shown by Anderson and Roble⁸, the spatial and temporal variability of F-layer densities near the magnetic equator can have dramatic effects on the neutral dynamics. We seek here to demonstrate typical differences in neutral wind structures implied by the more realistic FAIM than the widely used Chiu² empirical ionospheric model. To do this requires only a fairly simple model. At the geographic equator, the Coriolis force is zero and the following zonal momentum equation decouples from the meridional equation:

$$\frac{\delta u}{\delta t} = -\frac{1}{\rho} \frac{\delta p}{\delta x} - v p(u - u_p) + \frac{\mu}{\rho} \frac{\delta^2 u}{\delta z^2} \quad (11)$$

where

u = zonal (eastward) wind speed

t = local time

ρ = neutral mass density

p = neutral pressure

-
8. Anderson, D.N. and Roble, R.G. (1974) The effect of vertical $E \times B$ ionospheric drifts on F-region neutral winds in the low-latitude thermosphere, *J. Geophys. Res.* **79**:5231-5236.
 9. Anderson, D.N., Heelis, R.A., and McClure, J.P. (1987b) Calculated nighttime eastward plasma drift velocities at low latitudes and their solar cycle dependence, *Annal. Geophys.* **5A**(6):435-442.

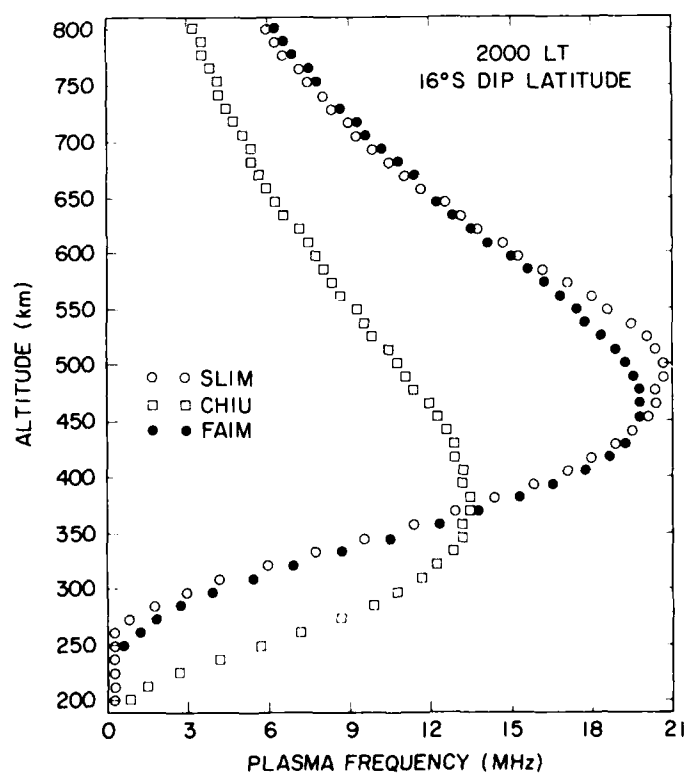
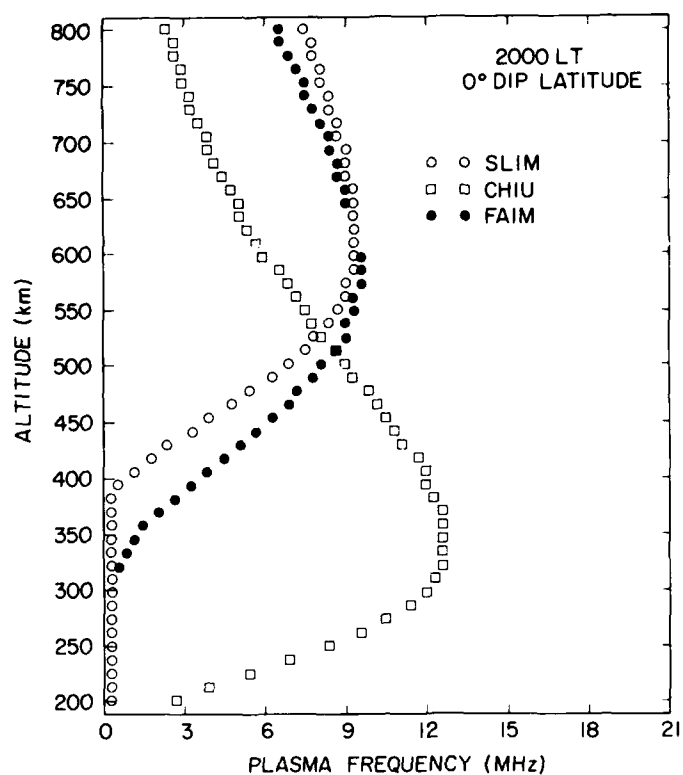


Figure 5. (a) Comparison Between SLIM, Chiu, and FAIM Electron Density Profiles at the Magnetic Equator at 2000 LT. (b) Same as (a), Except at 16°S Dip Latitude.

x = distance in zonal direction = Ωat
 Ω = earth's angular velocity
 a = earth's radius
 μ = molecular viscosity coefficient
 z = altitude
 v_p = plasma-neutral collision frequency
 u_p = plasma drift speed

Pressure gradients are calculated from the MSIS-83 model¹⁰ which is based heavily on AE-E data at low latitudes, and so should represent pressure gradients with reasonable accuracy, at least at low to moderate solar activity. A simple diurnal variation of zonal plasma drifts is assumed based on data from Jicamarca radar¹¹

$$u_p = 30 + 70 \cos \frac{\pi}{12} (t - 22) \quad (12)$$

in ms^{-1} where t = local time in hours.

Contours of eastward wind speed as a function of altitude (150 - 300 km) and local time (0 - 24 hours) are illustrated in Figures 6a and 6b during solar maximum conditions ($F_{10.7} = 185$) conditions for the Chiu and FAIM models, respectively. Figure 6c illustrates the differences between these two contour plots (FAIM minus Chiu), and represents the differences in neutral wind speed due to the differences in the two model plasma density distributions. Figure 4d similarly illustrates these difference fields for solar minimum ($F_{10.7} = 70$) conditions. One immediately notes, from the difference field contours, that the dynamical consequences of utilizing FAIM vs. CHIU only become apparent between about 1800-0200 LT at SS MAX, and 1300-2300 LT for SS MIN. In addition, the difference fields are positive at SS MAX and negative at SS MIN. There are several competing mechanisms that interplay to produce these results. First, the only significant differences in foF2 between FAIM and SLIM occur between 1200 LT and (1900 LT, 2200 LT) at (SS MIN, SS MAX), where the Chiu foF2s exceed those of SLIM by 2 - 3 MHz. Furthermore, during the daytime the neutral dynamics are considerably less sensitive to differences in hmF2, since the layer is very broad and the ion drag effect is distributed over a wide range of altitudes. Finally, the effects of ion drag are considerably less at the magnetic equator than at higher latitudes, since $v_p(u - u_p)$ is much smaller than $v_p u$, especially at night when u and u_p are interactively coupled via the F-layer dynamo mechanism.

Despite the above ameliorating factors, the difference fields shown in Figures 6c and 6d still represent a significant fraction of the total zonal wind. During both SS MIN and SS MAX, the Chiu model foF2s exceed those of FAIM by about 2 - 3 MHz between 1200 and 2100 LT. In addition, during SS MAX, hmF2s from FAIM so far exceed (by 100 - 150 km) those from Chiu² that the F-layer is essentially lifted up out of the region below 300 km; and the ion drag force is essentially eliminated, allowing u to accelerate to values of 160 - 200 ms^{-1} . During SS MIN the situation is quite different. The hmF2s given by Chiu and FAIM for the pre-/post-sunset period are very similar, and quite low

-
10. Hedin, A.E. (1983) A revised thermospheric model based on mass spectrometer and incoherent scatter data: MSIS-83, *J. Geophys. Res.* **88**:10170-10188.
 11. Fejer, B.G., Kudeki, W., and Farley, D.T. (1981) Equatorial F-region zonal plasma drifts, *J. Geophys. Res.* **90**:12249-12255.

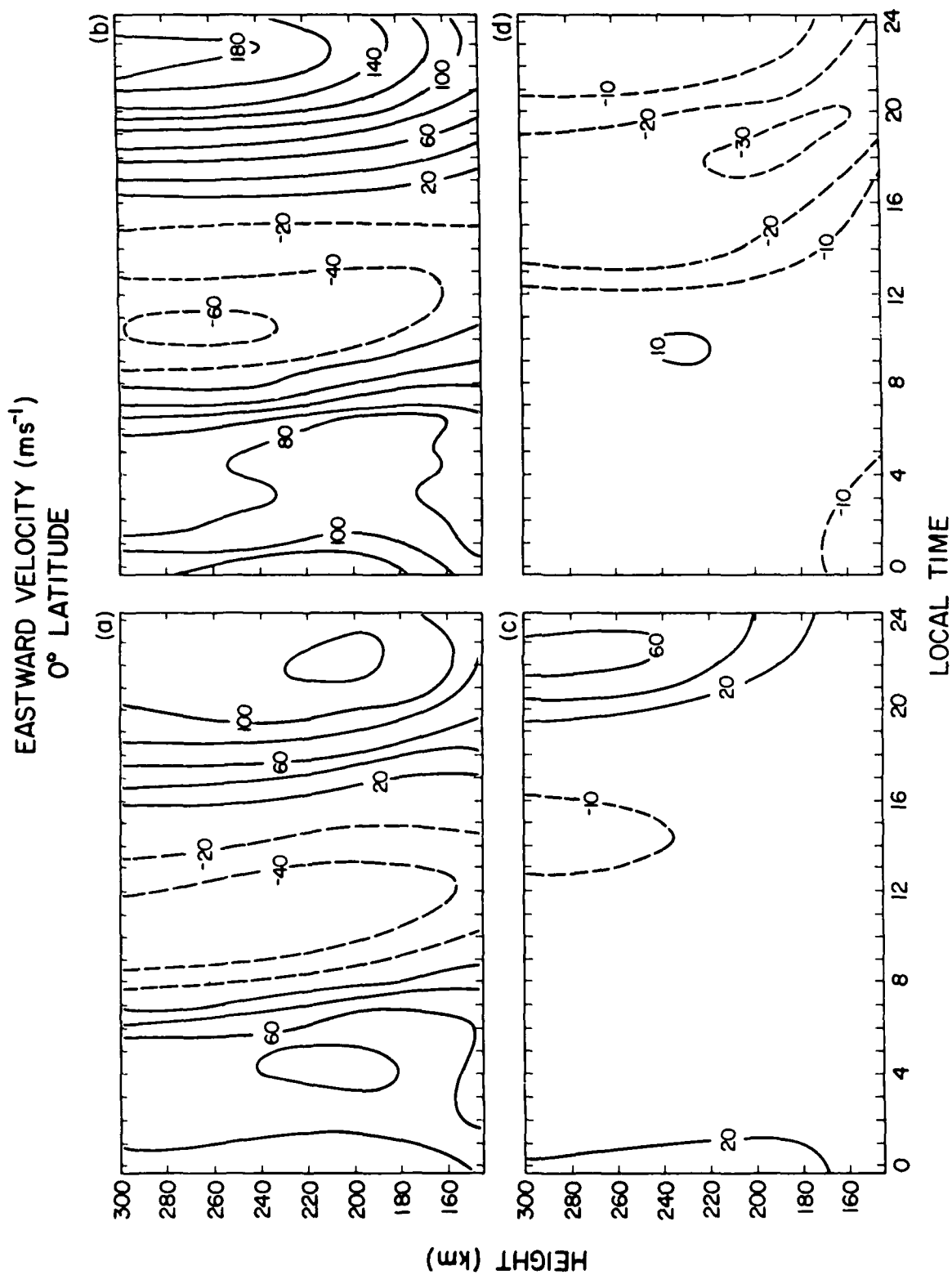


Figure 6. (a) Calculated Eastward Neutral Winds at the Equator for Solar Maximum Conditions Using the Chiu Plasma Density Model. (b) Same as (a), except for FAIM plasma density model. (c) Same as (a), except for solar maximum conditions. (d) Same as (c), except for solar minimum conditions.

(~300 km) as compared to SSMAX (~450 km). And, even though the Chiu foF2s exceed those of FAIM by 2 MHz, the much broader profile shape and, hence, larger height-integrated ion drag force given by FAIM leads to the negative difference fields in Figure 6d. Similarly important dynamical effects occur near the anomaly peaks (roughly $\pm 15^\circ$ geomagnetic latitude). One would therefore anticipate significant differences in the low-latitude thermosphere circulation pattern simulated with a 3-D general circulation model when using the more realistic FAIM model as opposed to Chiu², or in electrodynamic simulations of E-/F-region coupling involving field-aligned integrated conductivities.

References

1. Anderson, D.N., Mendillo, M., and Herniter, B. (1987a) A semi-empirical, low-latitude ionospheric model, *Radio Sci.* **22**:292-306.
2. Chiu, Y.T. (1975) An improved phenomenological model of ionospheric density, *J. Atmos. Terr.* **37**:1563-1570.
3. Llewellyn, S.K. and Bent, R.B. (1973) *Documentation and Description of the Bent Ionospheric Model*, AFCRL-TR-73-0657, AD 772733, Air Force Cambridge Research Laboratories, Bedford, MA.
4. Bradley, P.A. and Dudeney, J.R. (1973) A simple model of the vertical distribution of electron concentration in the ionosphere, *J. Atmos. Terr. Phys.* **35**:2131.
5. Rajaram, G. and Rastogi, R.G. (1977) Equatorial electron densities-seasonal and solar cycle changes, *J. Atmos. Terr. Phys.* **39**:1175-1182.
6. Rastogi, R.G. (1966) The equatorial anomaly in the F2 region of the ionosphere, *Inst. Telecomm. Engrs.* **12**:245-256.
7. Woodman, R.F. (1970) Vertical drift velocities and east-west electric fields at the magnetic equator, *J. Geophys. Res.* **75**:6249-6259.
8. Anderson, D.N. and Roble, R.G. (1974) The effect of vertical $E \times B$ ionospheric drifts on F-region neutral winds in the low-latitude thermosphere, *J. Geophys. Res.* **79**:5231-5236.
9. Anderson, D.N., Heelis, R.A., and McClure, J.P. (1987b) Calculated nighttime eastward plasma drift velocities at low latitudes and their solar cycle dependence, *Annal. Geophys.* **5A(6)**:435-442.
10. Hedin, A.E. (1983) A revised thermospheric model based on mass spectrometer and incoherent scatter data: MSIS-83, *J. Geophys. Res.* **88**:10170-10188.
11. Fejer, B.G., Kudeki, W., and Farley, D.T. (1981) Equatorial F-region zonal plasma drifts, *J. Geophys. Res.* **86**:12249-12255.

Appendix A

**Latitude Variation in the Diurnal, Semidiurnal and Terdiurnal Phase and
Amplitude Components of hmF2 and foF2 in Three Longitude Sectors
during September 1984**

Table 1. Ionosonde Stations Utilized for Data Depicted in Figures A1-A14
September, 1984

<u>Station</u>	<u>Geographic Lat. Long</u>	<u>Geomagnetic Lat. Long</u>
Kergulen	-49.3, +70.2	-57.4, +129.9
La Reunion	-21.2, +55.6	-27.4, +121.5
Tahiti	-17.7, +210.7	-15.2, +284.4
Manila	+14.7, +121.1	+3.6, +191.1
Chung-Li	+24.9, +121.2	+13.6, +189.5
Okinawa	+26.3, +127.8	+15.5, -163.1
Ouagadougou	+12.4, +358.5	+16.2, +71.6
Yamagawa	+31.2, +130.6	+20.6, -160.9
Maui	+20.8, +203.5	+21.2, +269.6
Dakar	+14.8, +342.6	+21.4, +56.0
Kokubungi-Tokyo	+35.7, +139.5	+25.7, -153.3
Akita	+39.7, +140.1	+29.8, -153.2
Tashkent	+41.3, +69.6	+32.3, +145.2
Alma Ata	+43.3, +76.9	+33.5, +151.9
Wakkanai	+45.4, +141.7	+35.5, -152.7
Khabarousk	+48.5, +135.1	+38.1, -158.7
Karaganda	+49.8, +73.1	+40.3, +149.8
Irkutsk	+52.5, +104.0	+41.2, +175.5
Rome	+41.8, +12.5	+42.3, +93.2
Pt. Arguello	+35.6, +239.4	+42.3, +302.4
Novosibirsk	+54.6, +83.2	+44.2, +158.9
Bekescsaba	+46.7, +21.2	+45.2, +103.2
Tomsk	+56.5, +84.9	+46.0, +160.6
Kiev	+50.5, +30.5	+47.1, +113.3
Boulder	+40.0, +254.7	+48.9, +318.2
Poitiers	+46.6, +0.3	+49.2, +83.0
Wallops	+37.8, +284.5	+49.2, +353.9
Gorky	+56.2, +44.3	+50.2, +127.7
Moscow	+55.5, +39.3	+50.4, +123.2
Dourbes	+50.1, +4.6	+51.7, +88.9
Lannion	+48.8, +356.5	+52.0, +80.1
Kaliningrad	+54.7, +20.6	+53.0, +106.4
Slough	+51.5, +359.4	+54.0, +70.1
Juliusruh	+54.6, +13.4	+54.3, +99.7
Leningrad	+60.0, +30.7	+56.1, +118.3
Ottawa	+45.1, +283.9	+56.3, +352.7
Salekhard	+66.5, +66.5	+57.4, +149.7
Nurmijarvi	+60.5, +24.6	+57.7, +113.5
Uppsala	+59.8, +17.6	+58.3, +106.9
Arkhangelsk	+64.4, +40.5	+58.7, +129.1
Lycksele	+64.6, +18.7	+62.5, +111.7
Loparskaya	+68.0, +33.0	+63.1, +126.3
Sodankyla	+67.4, +26.6	+63.6, +120.8
Kiruna	+67.8, +20.4	+65.1, +116.4
Godhavn	+69.3, +306.5	+79.6, +34.7
Resolute Bay	+74.7, +83.2	+83.2, +292.9

hmF2

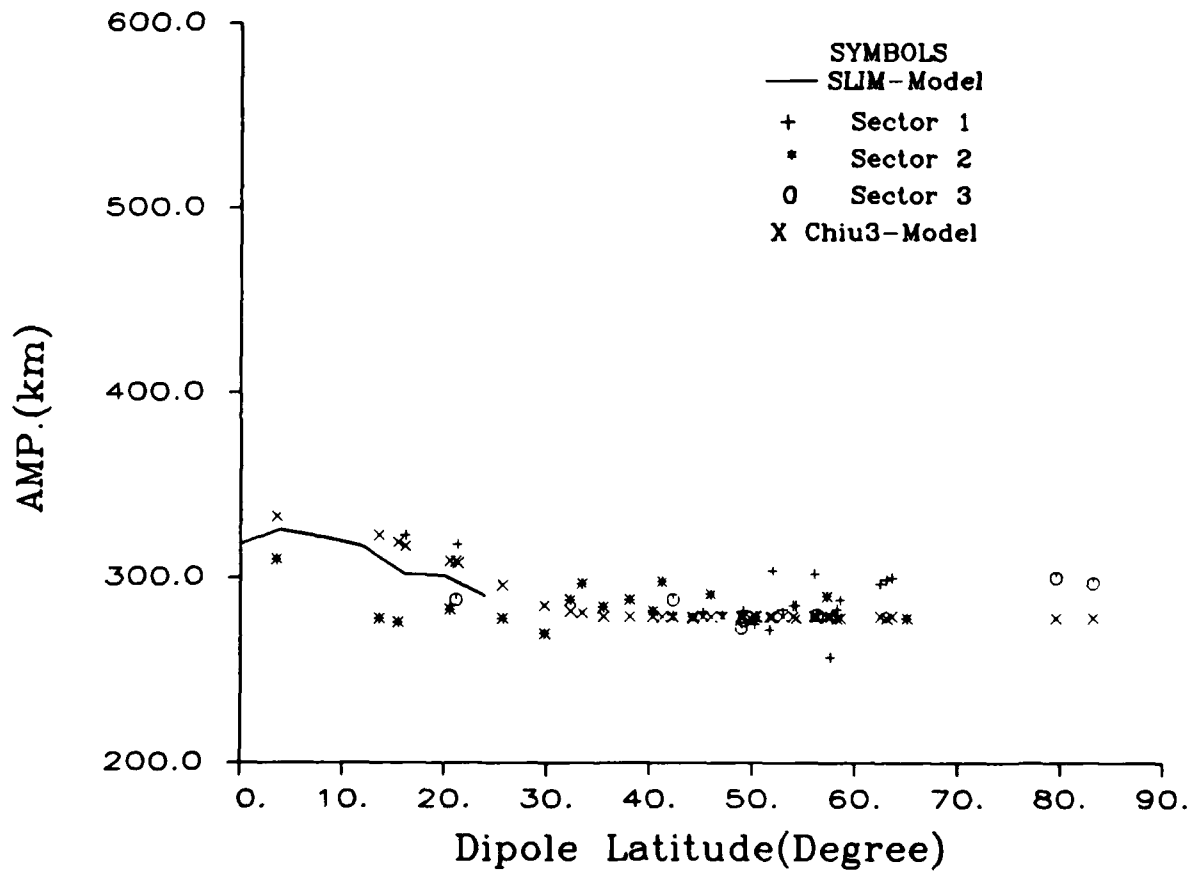


Figure A1. Diurnal and monthly mean hmF2's from ionosonde stations in the three longitude sectors, Sector 1: Europe, Africa, W. Asia; Sector 2: E. Asia, Pacific; Sector 3: America, Greenland, during September, 1984, and compared to the SLIM and FAIM models.

hmF2

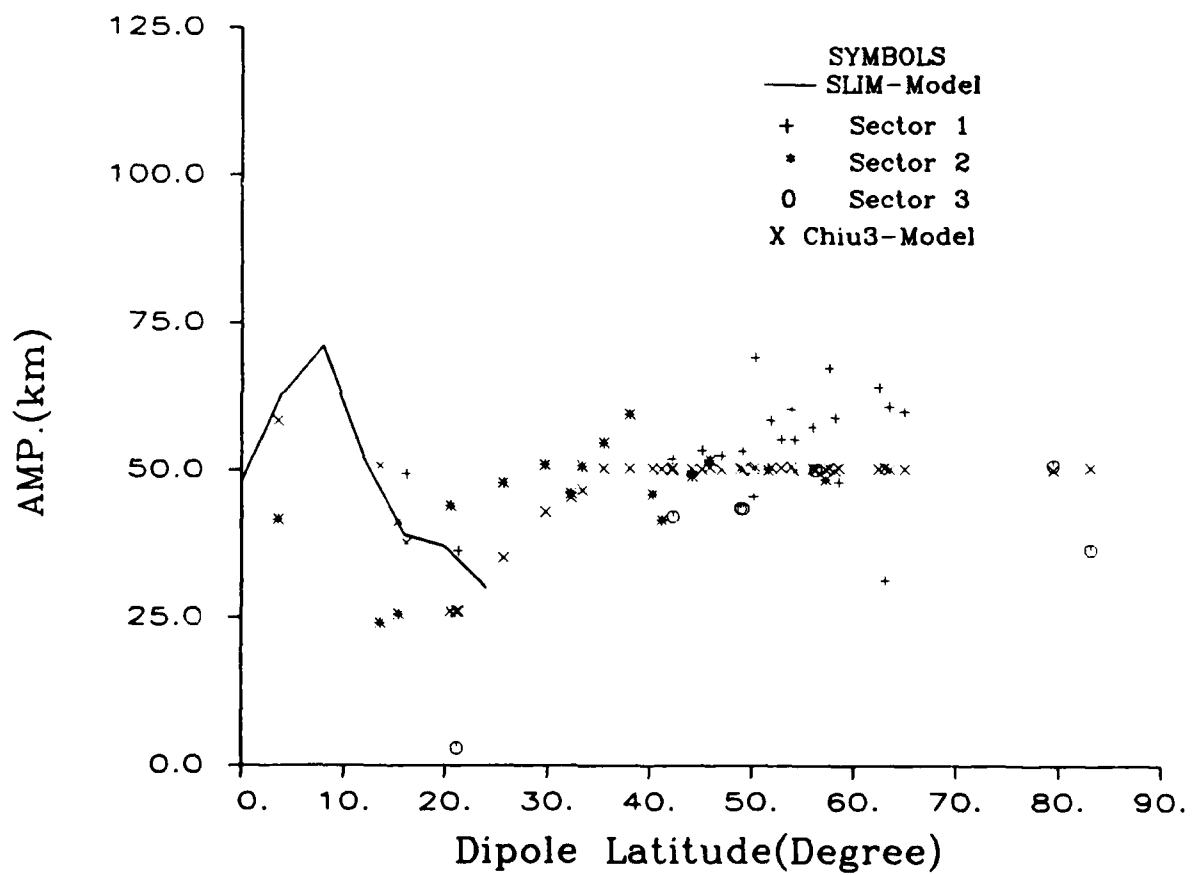


Figure A2. Same as A1, Except for Diurnal Amplitude.

hmF2

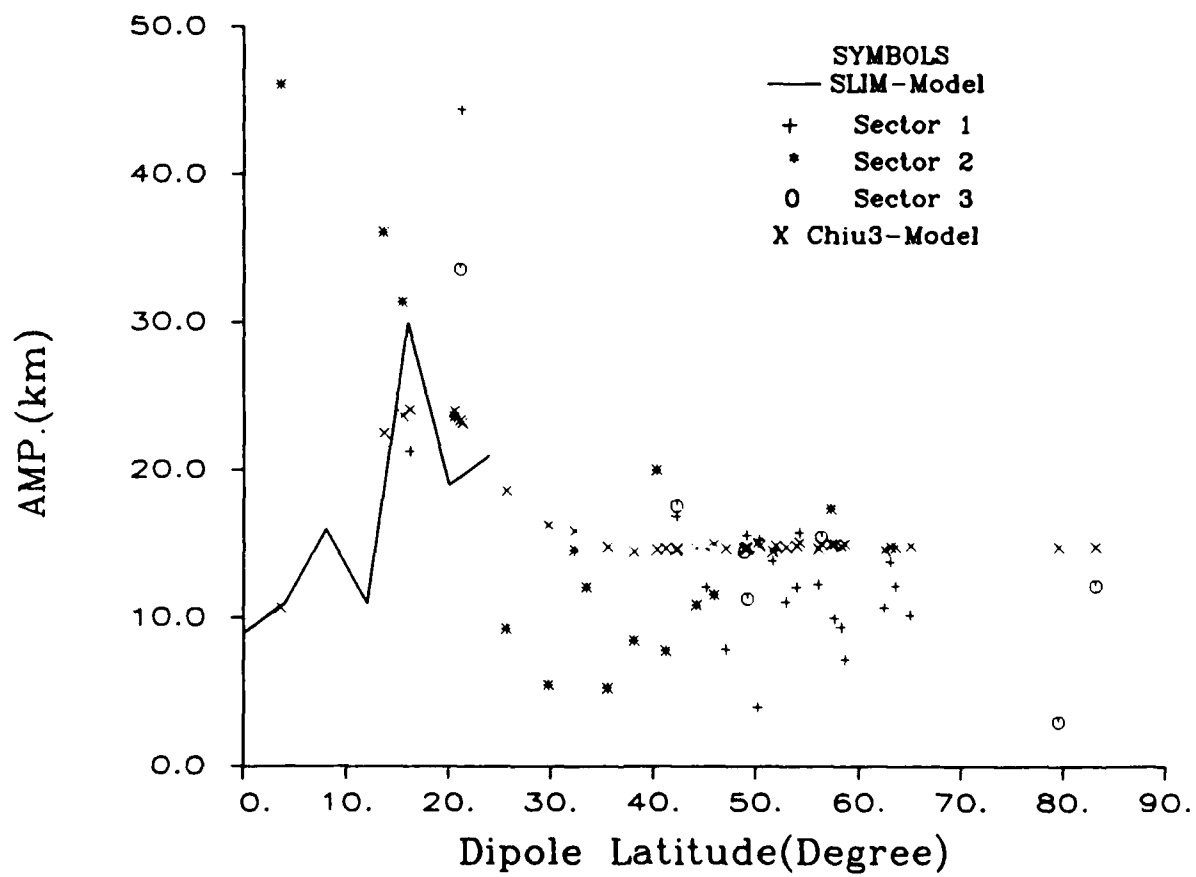


Figure A3. Same as A1, Except for Semidiurnal Amplitude.

hmF2

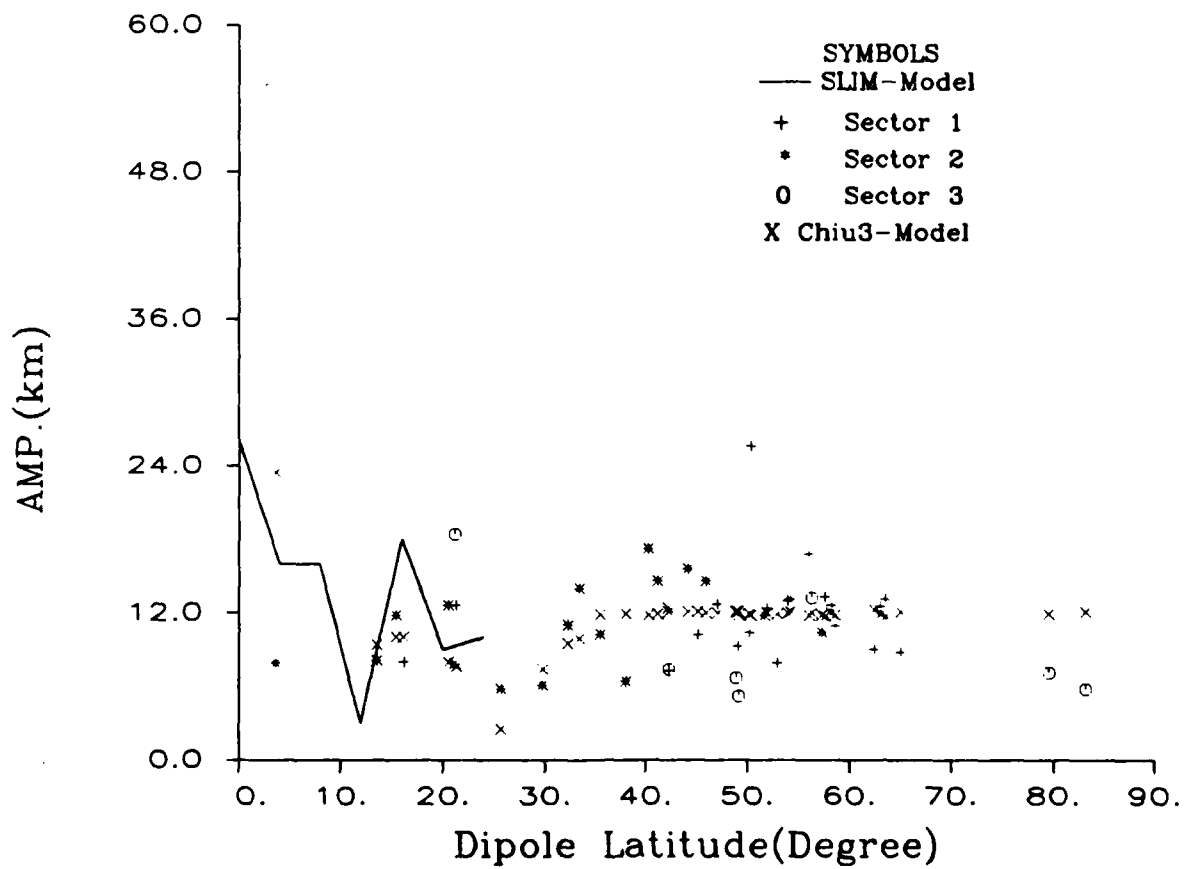


Figure A4. Same as A1, Except for Terdturnal Amplitude.

hmF2

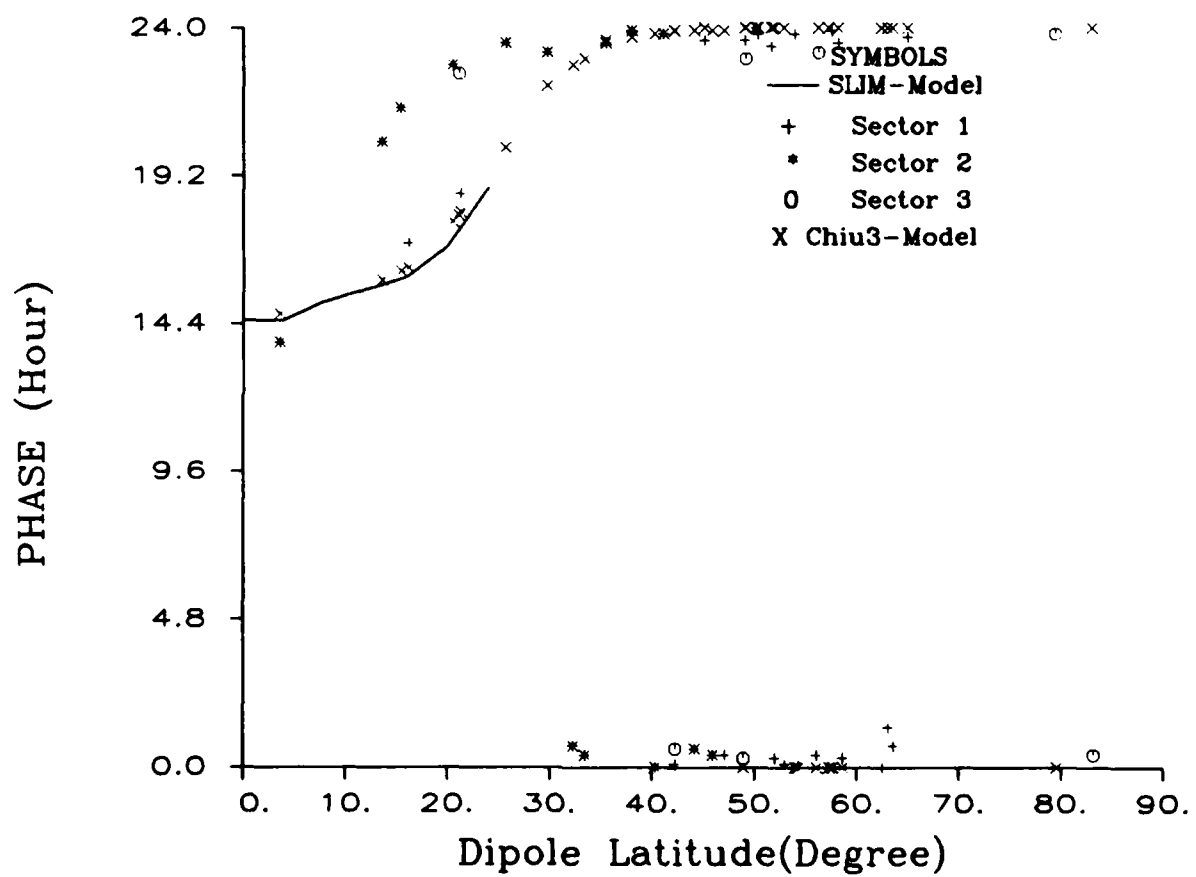


Figure A5. Same as A1, Except for Diurnal Phase.

hmF2

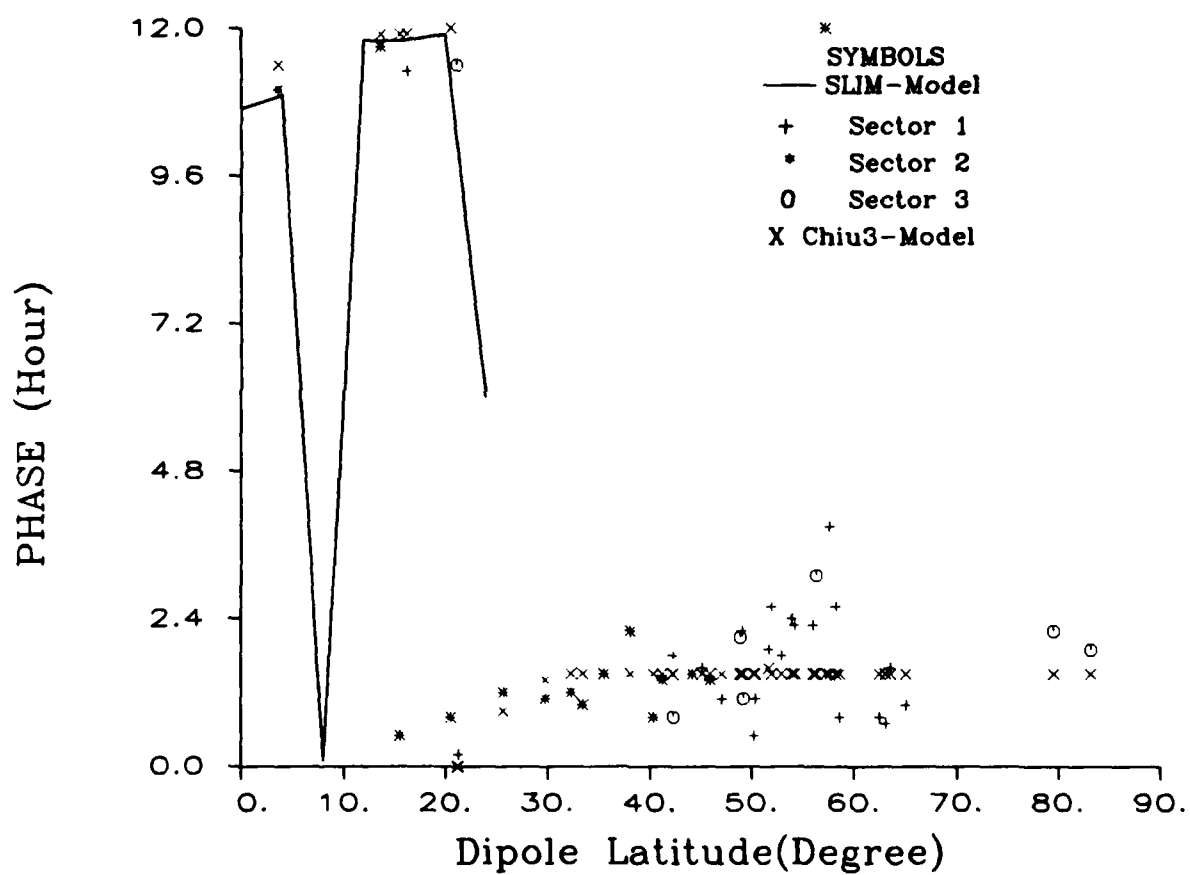


Figure A6. Same as A1, Except for Semidiurnal Phase.

hmF2

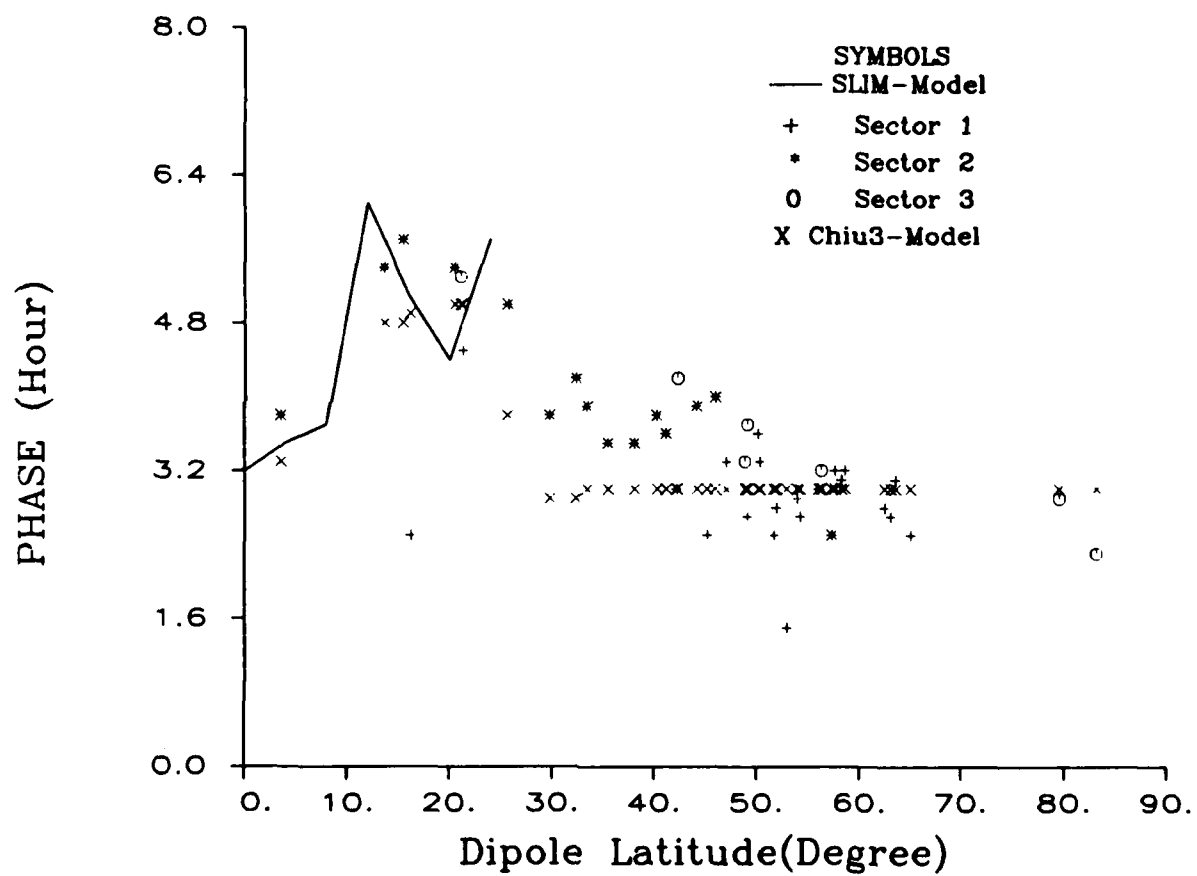


Figure A7. Same as A1, Except for Terdiurnal Phase.

foF2

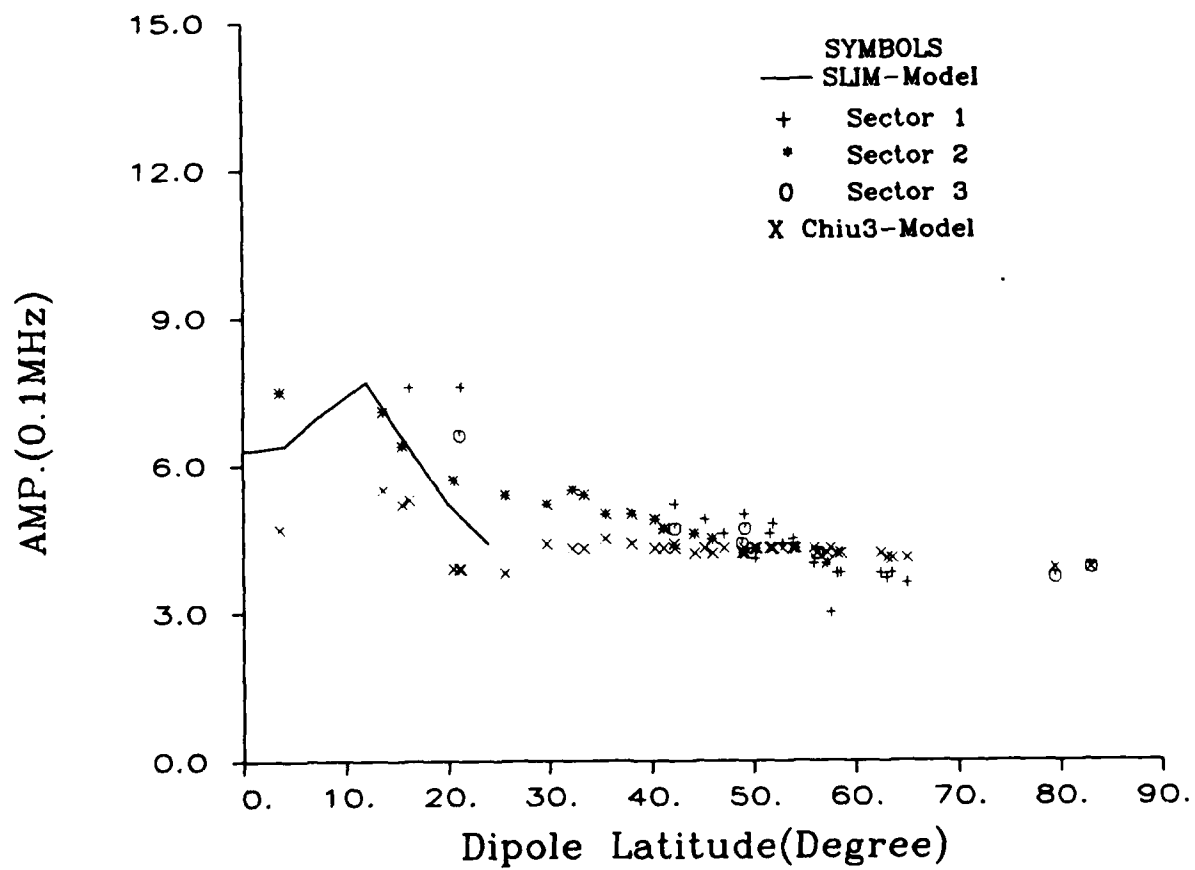


Figure A8. Same as A1, Except for foF2.

foF2

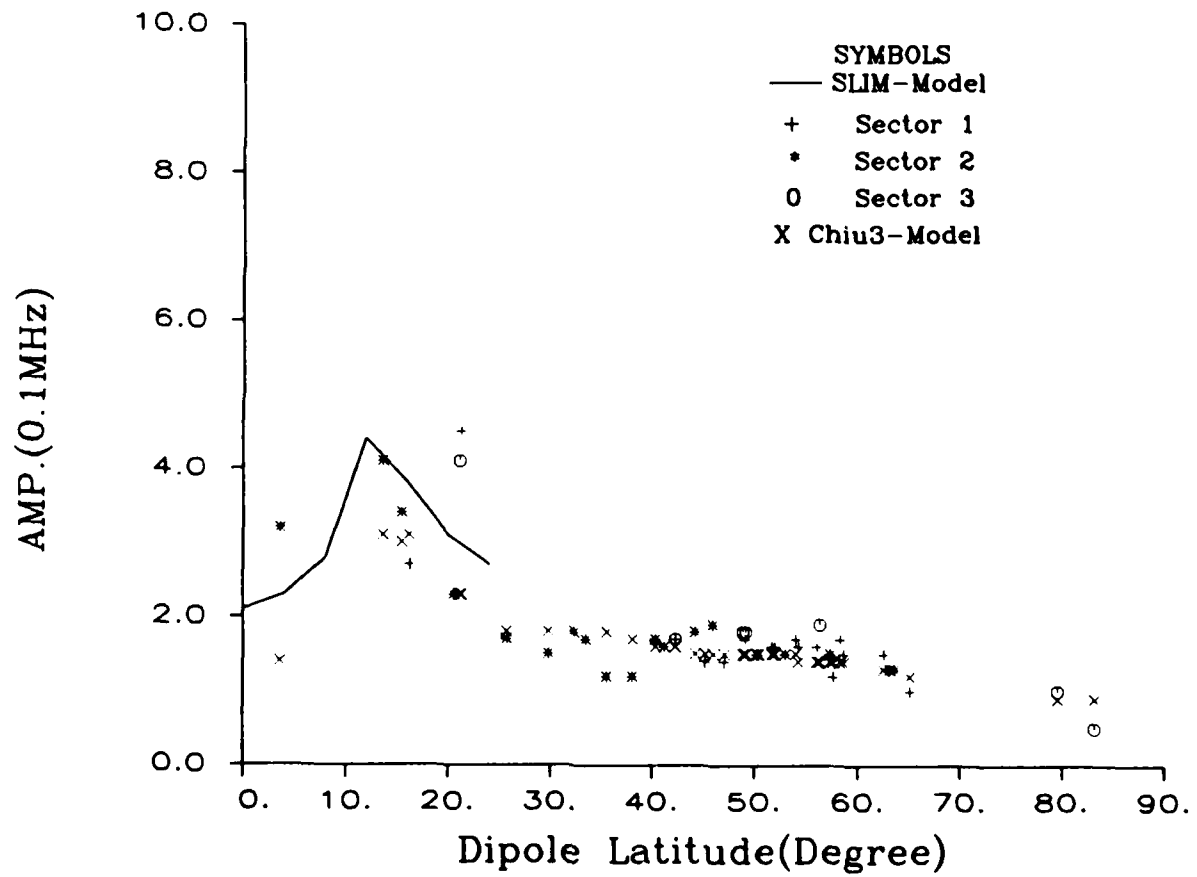


Figure A9. Same as A2, Except for foF2.

foF2

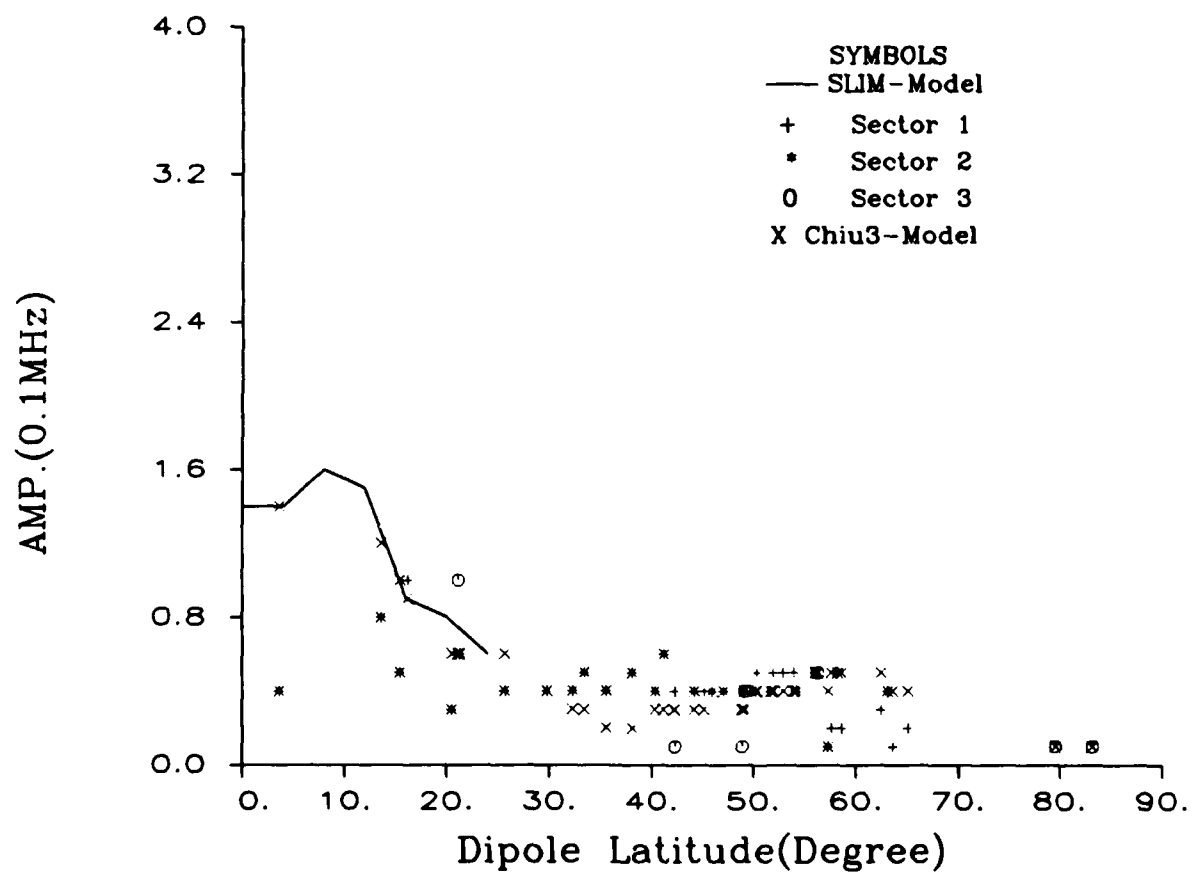


Figure A10. Same as A3, Except for foF2.

foF2

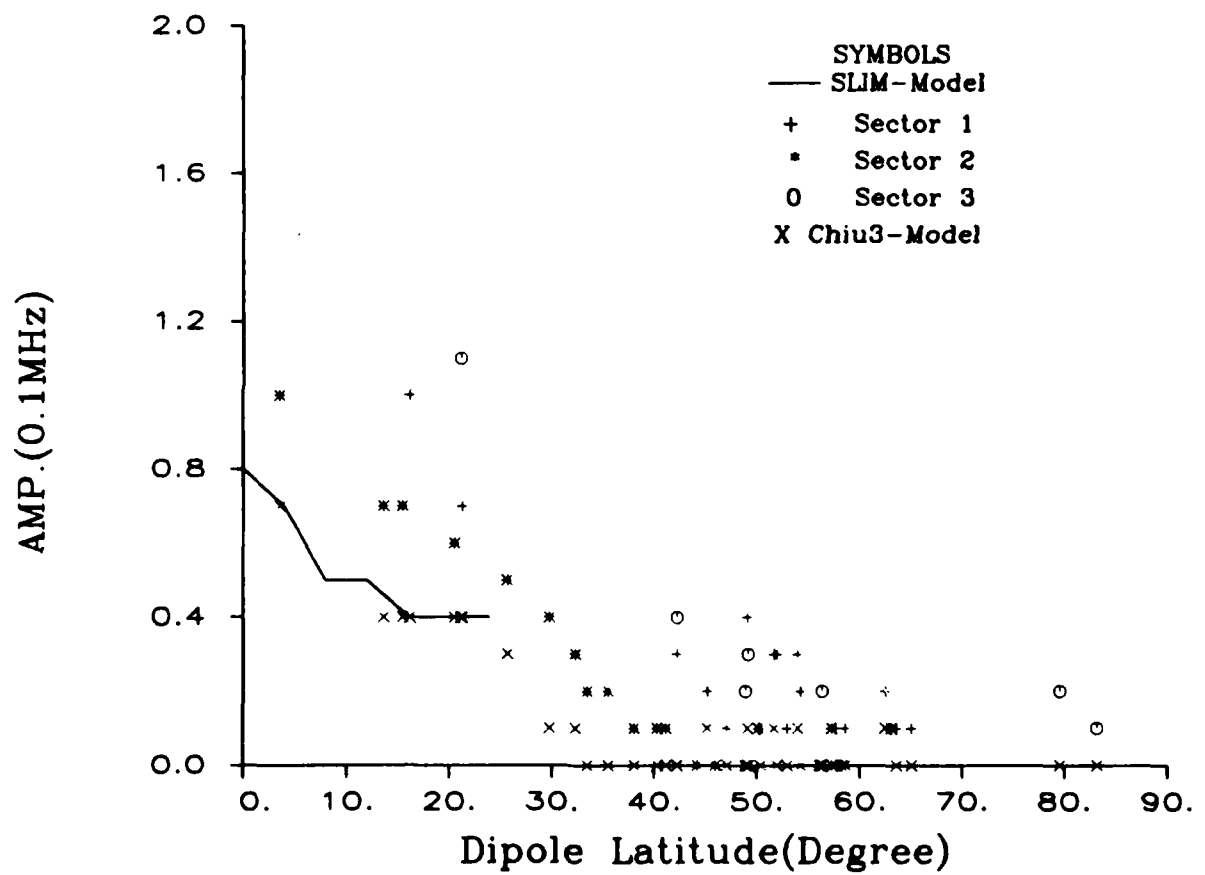


Figure A11. Same as A4, Except for foF2.

foF2

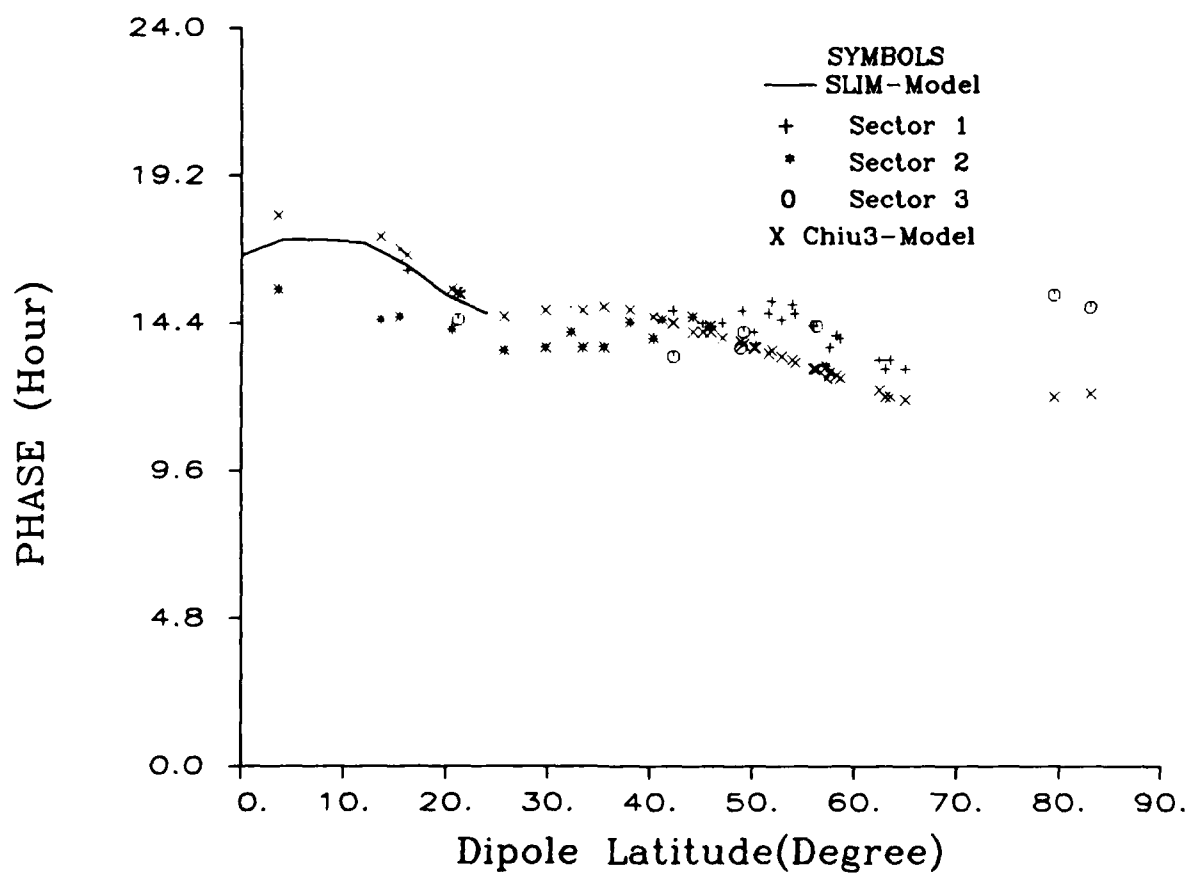


Figure A12. Same as A5, Except for foF2.

foF2

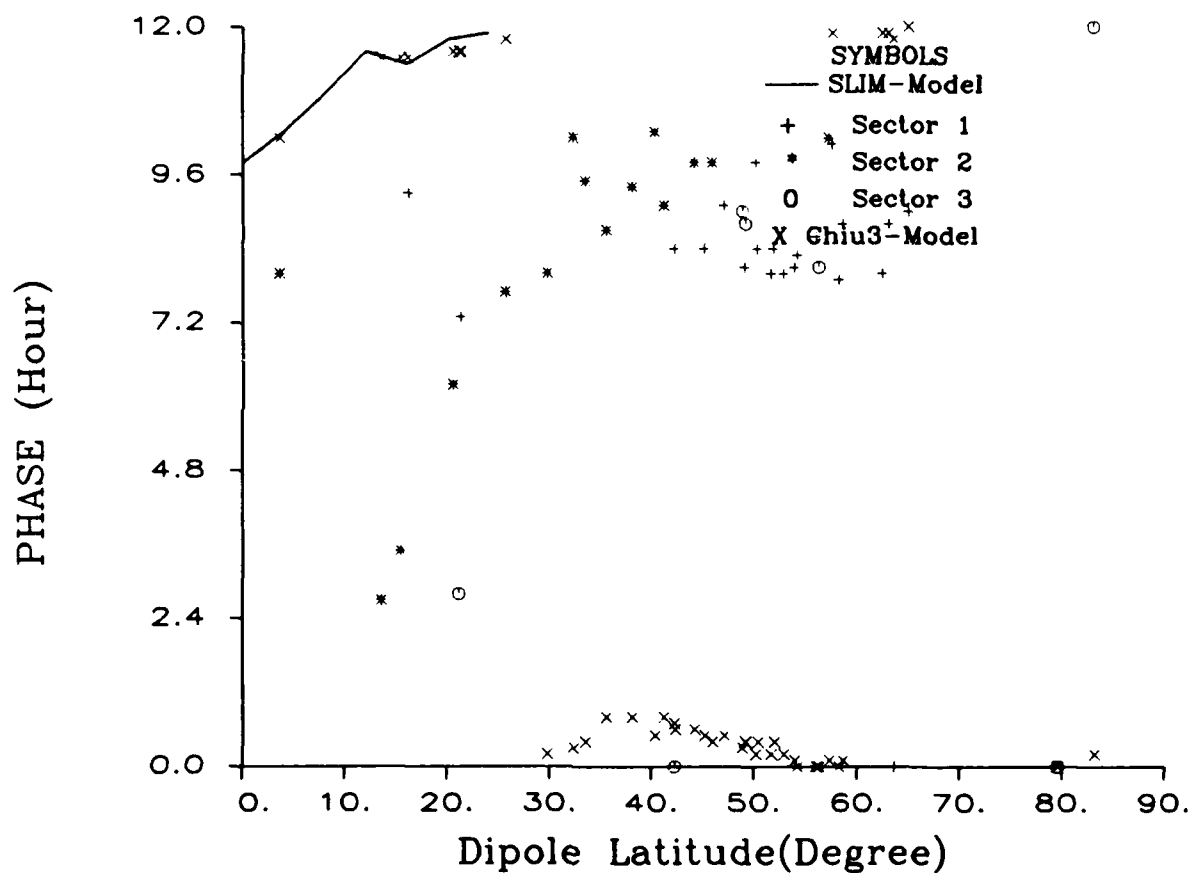


Figure A13. Same as A6, Except for foF2.

foF2

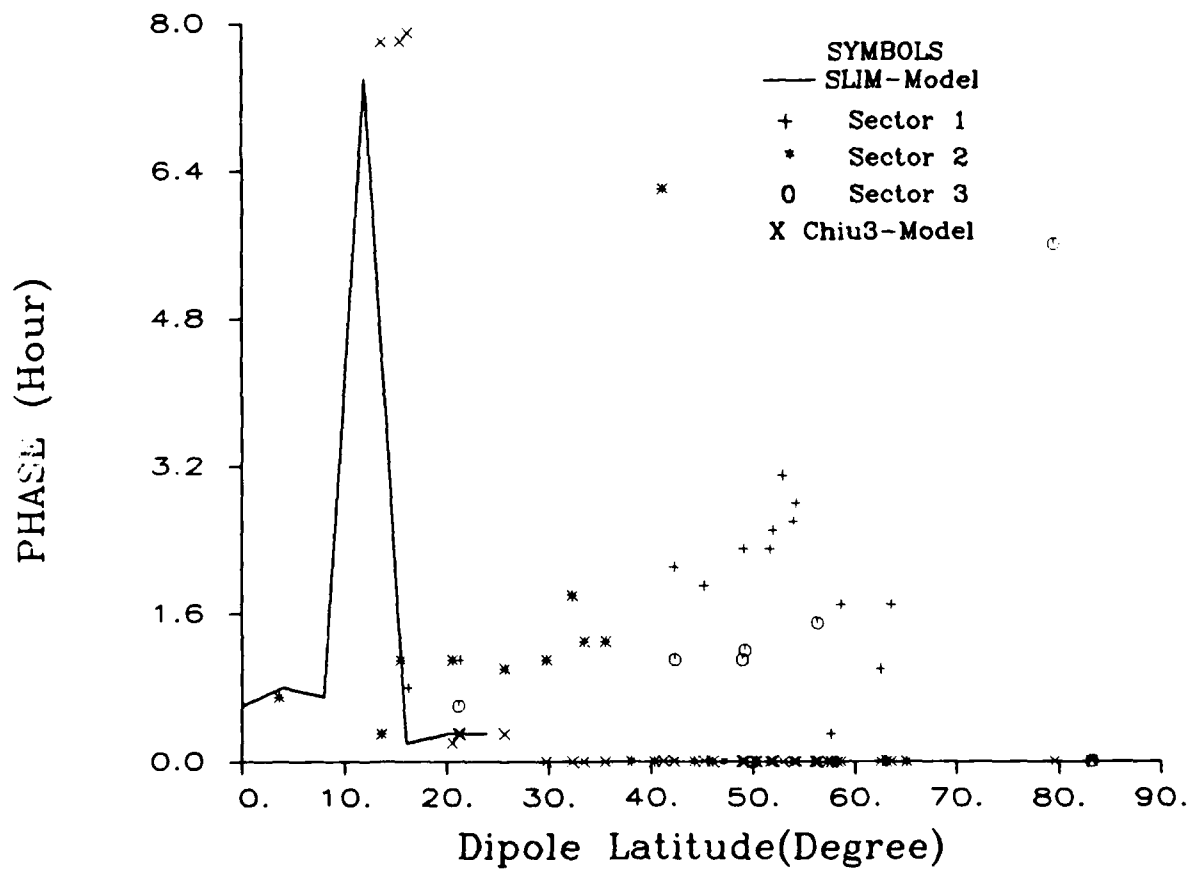


Figure A14. Same as A7, Except for foF2.

Appendix B

**Latitude Variation in the Diurnal, Semidiurnal and Terdiurnal Phase and
Amplitude Components of hmF2 and foF2 in Three Longitude Sectors
during March 1979**

Table 2. Ionosonde Stations Utilized for Data Depicted in Figures B1-B14
March, 1979

<u>Station</u>	<u>Geographic Lat. Long</u>	<u>Geomagnetic Lat. Long</u>
Bankok	+13.8, +100.6	+2.6, +169.9
Manila	+14.7, +121.1	+3.6, +191.1
Djibouti	+11.5, +42.8	+6.9, +114.9
Chung-Li	+24.9, +121.2	+13.6, +189.5
Okinawa	+26.3, +127.8	+15.5, -163.1
Ouagadougou	+12.4, +358.5	+16.2, +71.6
Yamagawa	+31.2, +130.6	+20.6, -160.9
Maul	+20.8, +203.5	+21.2, +269.6
Kokubungi-Tokyo	+35.7, +139.5	+25.7, -153.3
Seoul	+37.2, +126.6	+26.3, +195.0
Mexico	+19.3, +260.6	+29.0, +328.4
Akita	+39.7, +140.1	+29.8, -153.2
Wakkanai	+45.4, +141.7	+35.5, -152.7
White Sands	+32.3, +253.5	+41.2, +318.6
Rome	+41.8, +12.5	+42.3, +93.2
Pt. Arguello	+35.6, +239.4	+42.3, +302.4
Tomsk	+56.5, +84.9	+46.0, +160.6
Boulder	+40.0, +254.7	+48.9, +318.2
Poitiers	+46.6, +0.3	+49.2, +83.0
Wallops	+37.8, +284.5	+49.2, +353.9
Miedzeszyn	+52.2, +21.2	+50.5, +105.7
Yakutsk	+62.0, +129.6	+51.2, +194.9
Dourbes	+50.1, +4.6	+51.7, +88.9
Lindau	+51.7, +10.1	+52.1, +95.0
Lannion	+48.8, +356.5	+52.0, +80.1
Slough	+51.5, +359.4	+54.0, +70.1
Juliusruh	+54.6, +13.4	+54.3, +99.7
De Bilt	+52.1, +5.2	+53.5, +90.5
Ottawa	+45.1, +283.9	+56.3, +352.7
Nurmijarvi	+60.5, +24.6	+57.7, +113.5
Uppsala	+59.8, +17.6	+58.3, +106.9
Lycksele	+64.6, +18.7	+62.5, +111.7
Sodankyla	+67.4, +26.6	+63.6, +120.8
Kiruna	+67.8, +20.4	+65.1, +116.4
Resolute Bay	+74.7, +83.2	+83.2, +292.9

hmF2

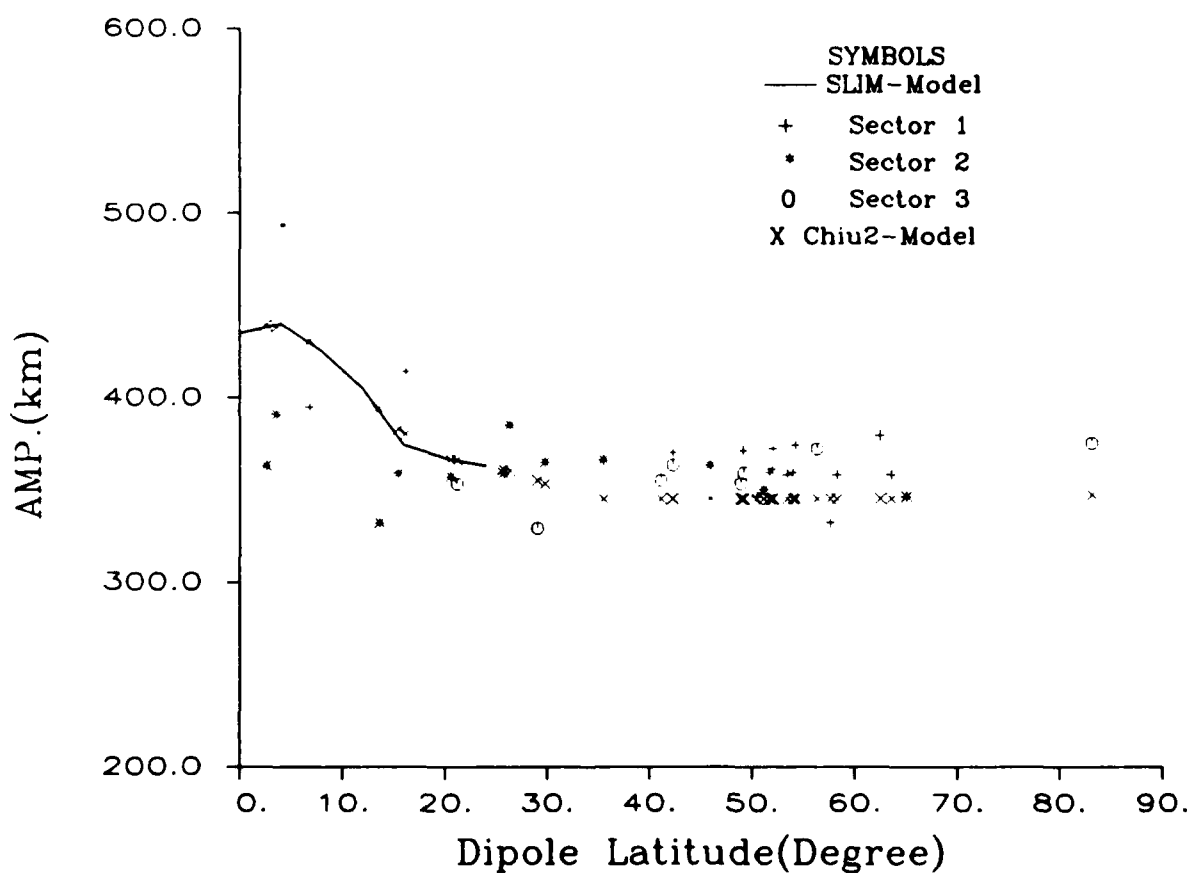


Figure B1. Diurnal and monthly mean hmF2's from ionosonde stations in the three longitude sectors, Sector 1: Europe, Africa, W. Asia; Sector 2: E. Asia, Pacific; Sector 3: America, Greenland, during March, 1979, and compared to the SLIM and FAIM models.

hmF2

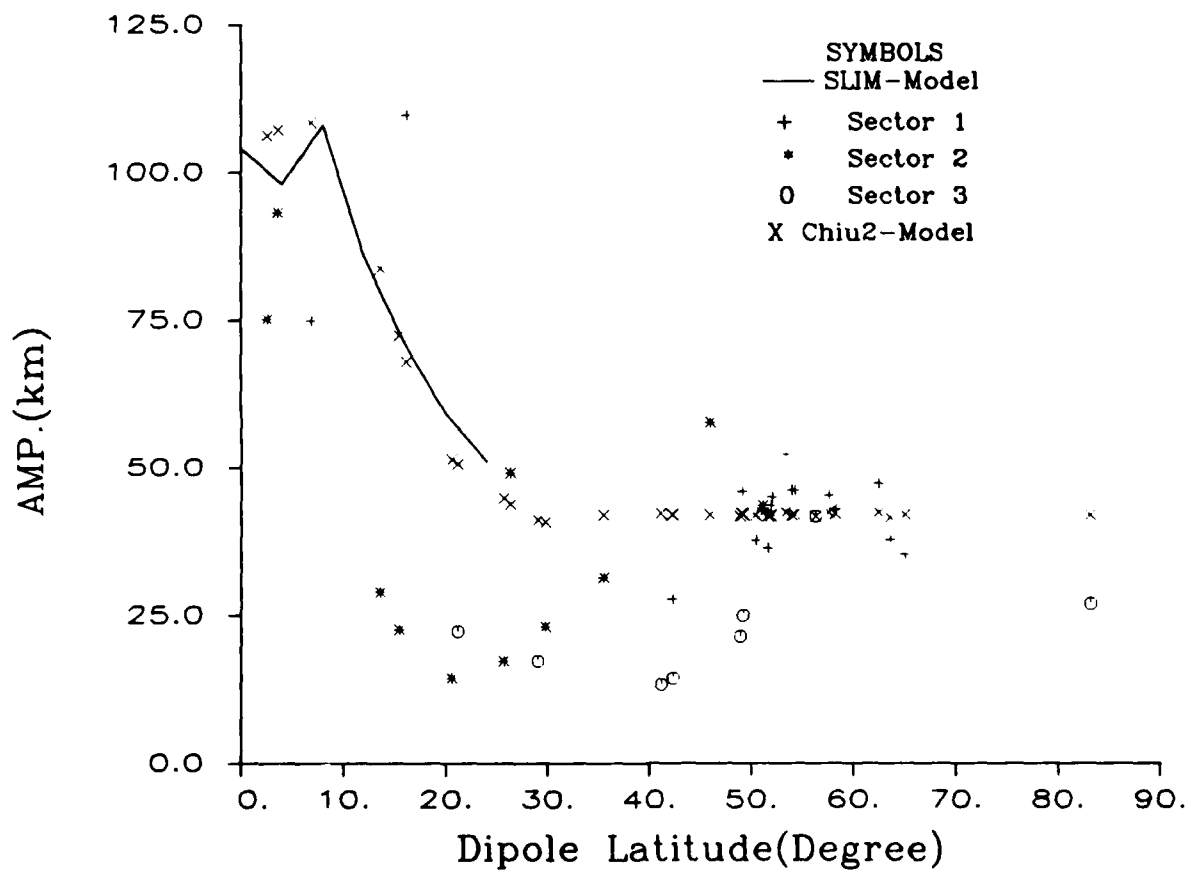


Figure B2. Same as B1, Except for Diurnal Amplitude.

hmF2

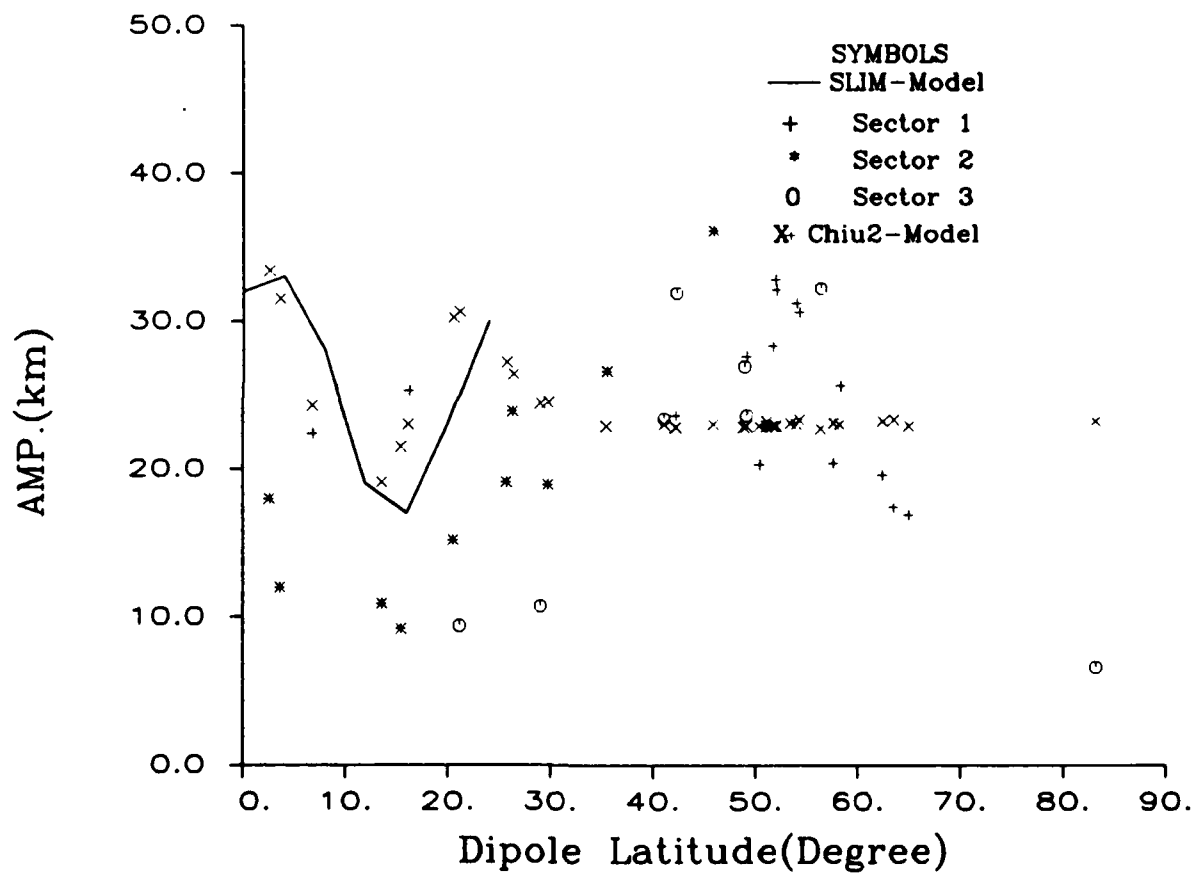


Figure B3. Same as B1, Except for Semidiurnal Amplitude.

hmF2

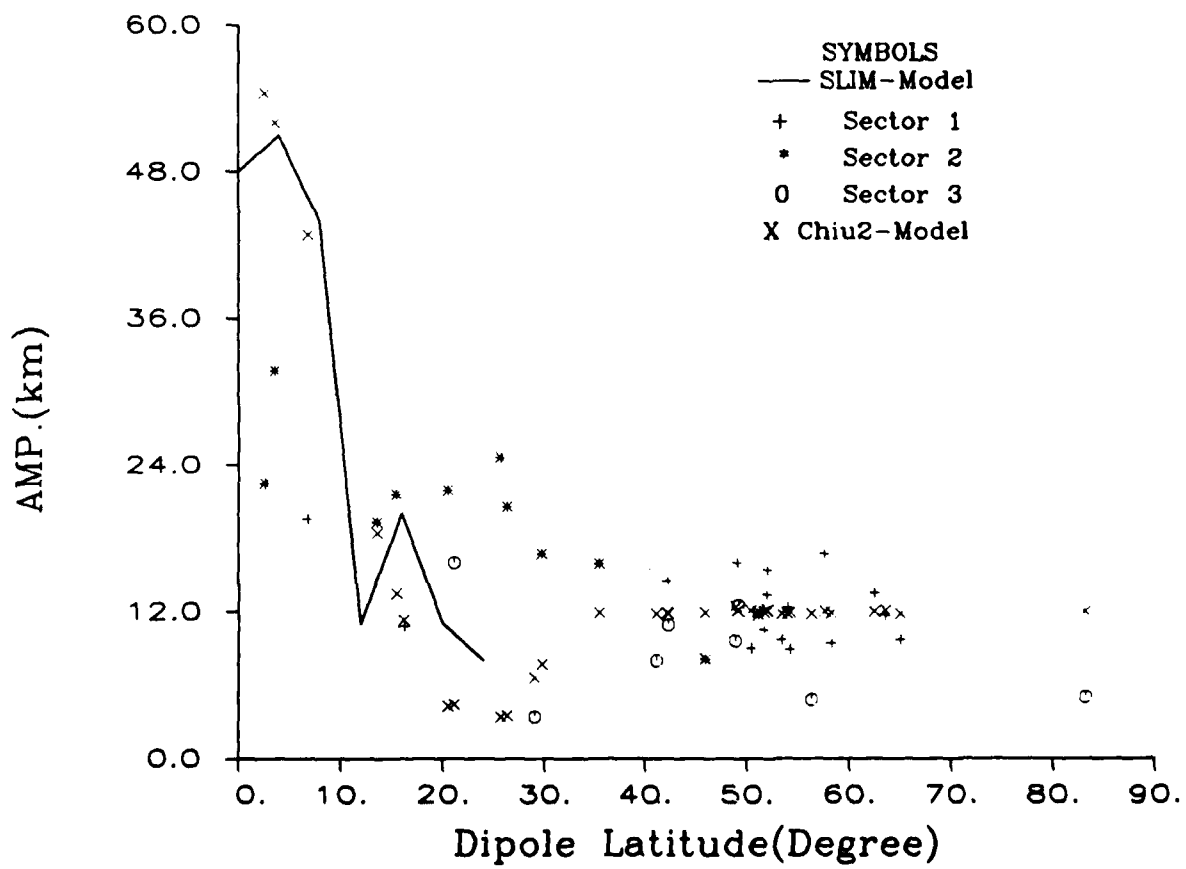


Figure B4. Same as B1, Except for Terdiurnal Amplitude.

hmF2

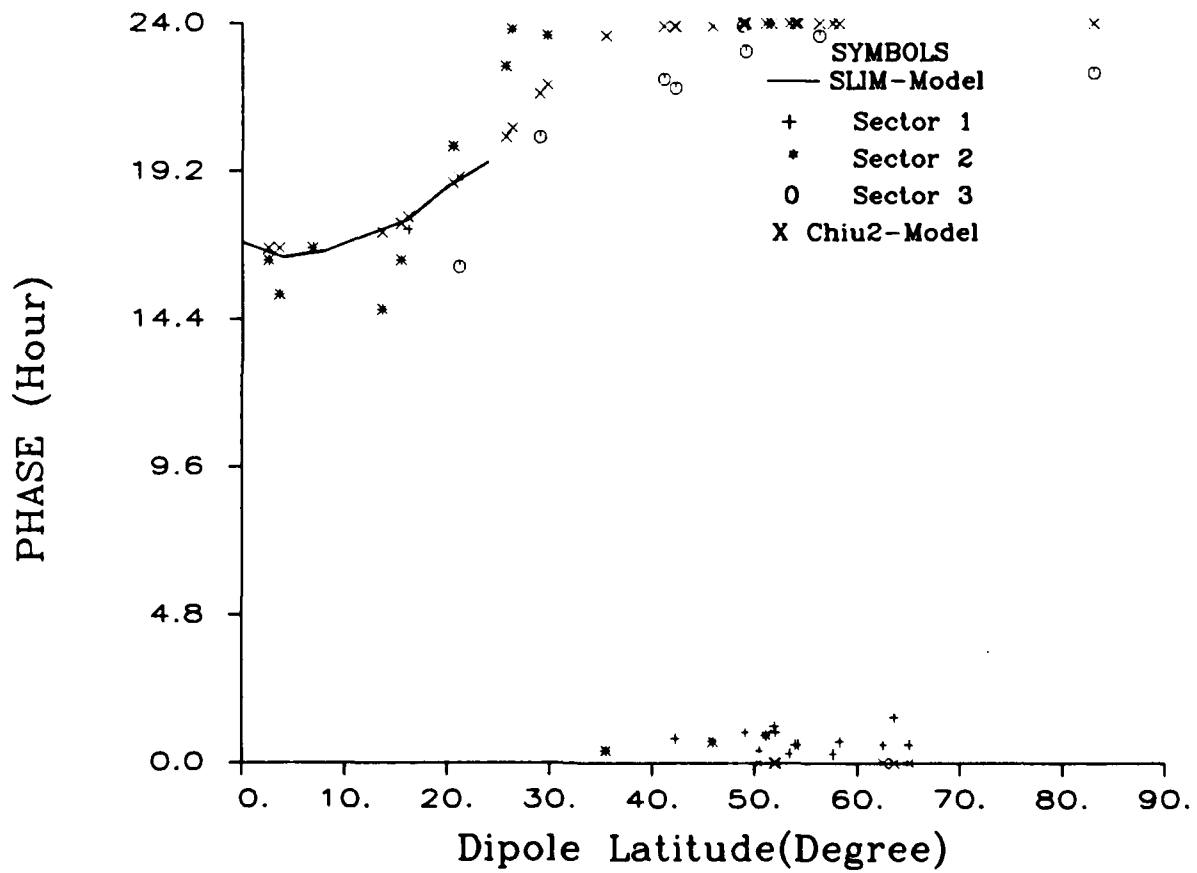


Figure B5. Same as B1, Except for Diurnal Phase.

hmF2

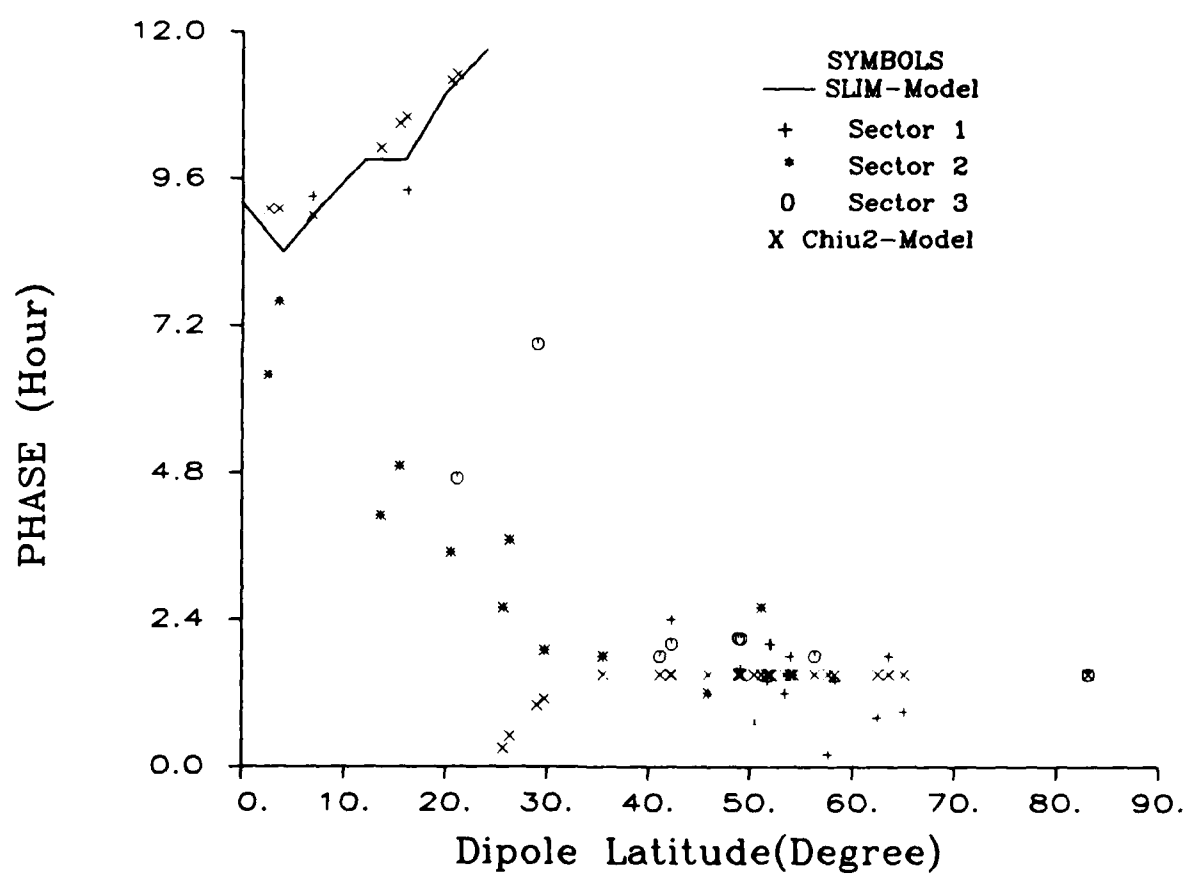


Figure B6. Same as B1, Except for Semidurnal Phase.

hmF2

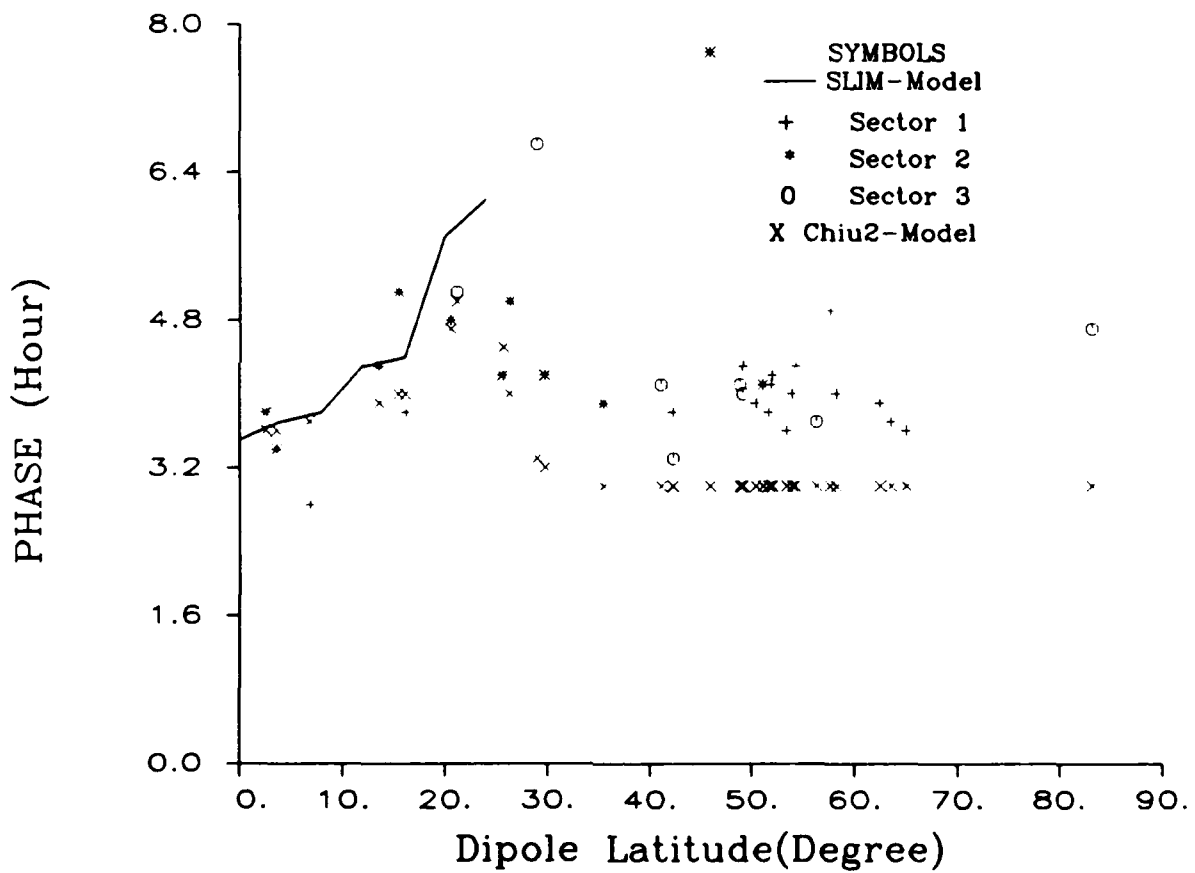


Figure B7. Same as B1, Except for Terdiurnal Phase.

foF2

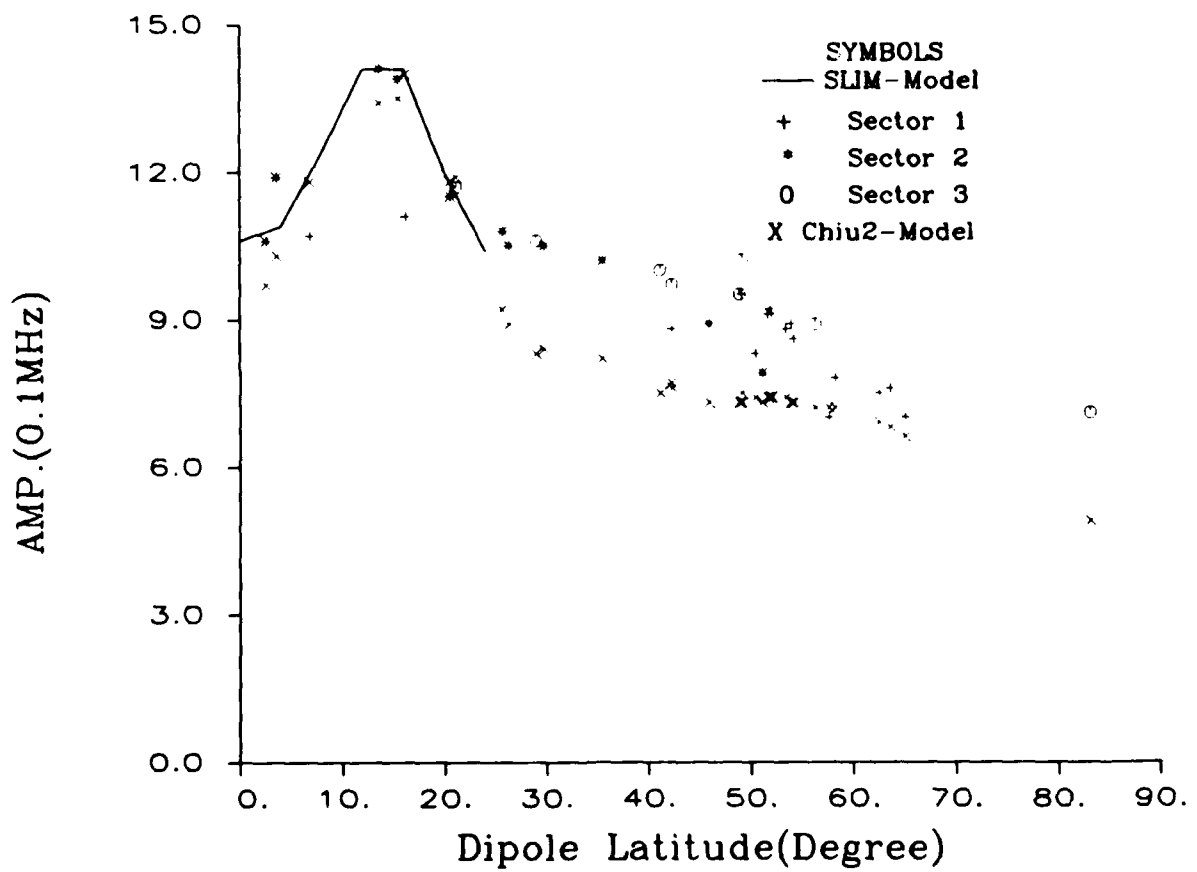


Figure B8. Same as B1, Except for foF2.

foF2

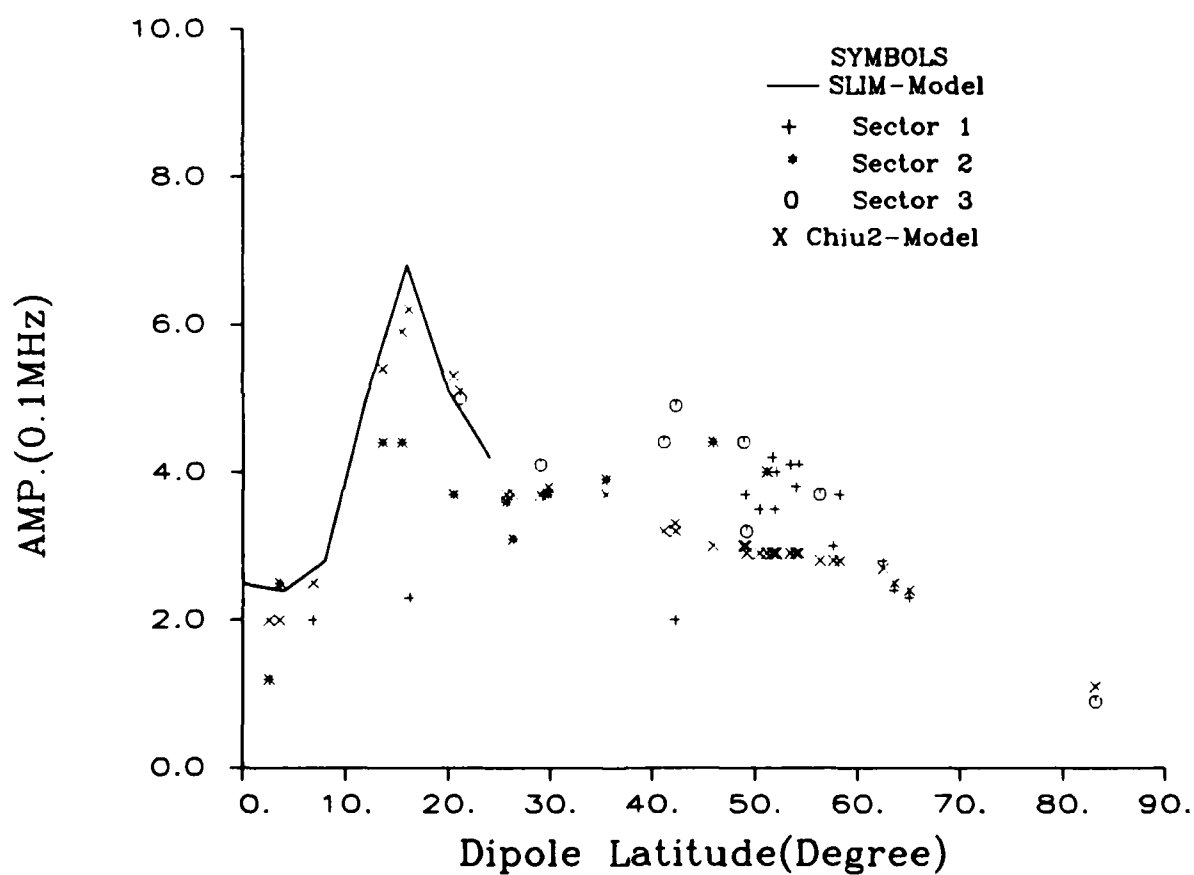


Figure B9. Same as B2, Except for foF2.

foF2

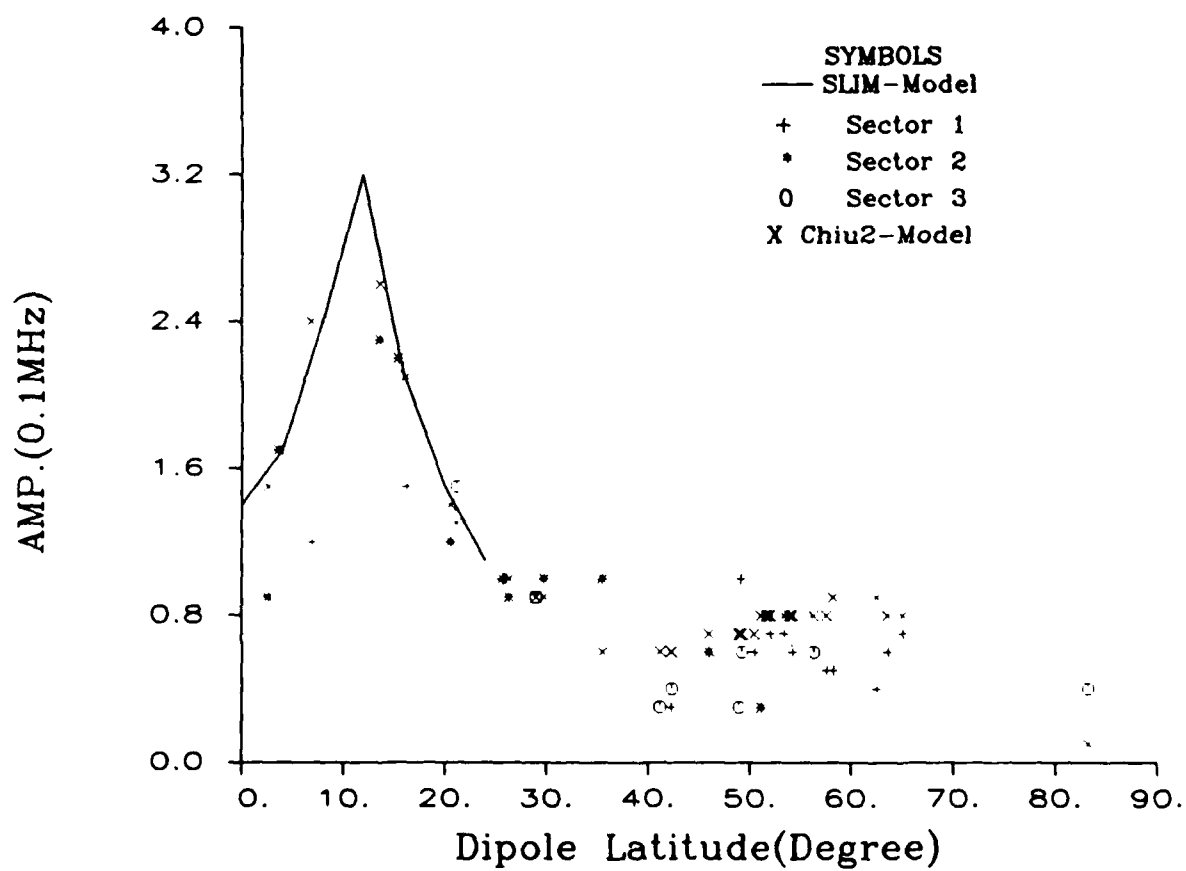


Figure B10. Same as B3, Except for foF2.

foF2

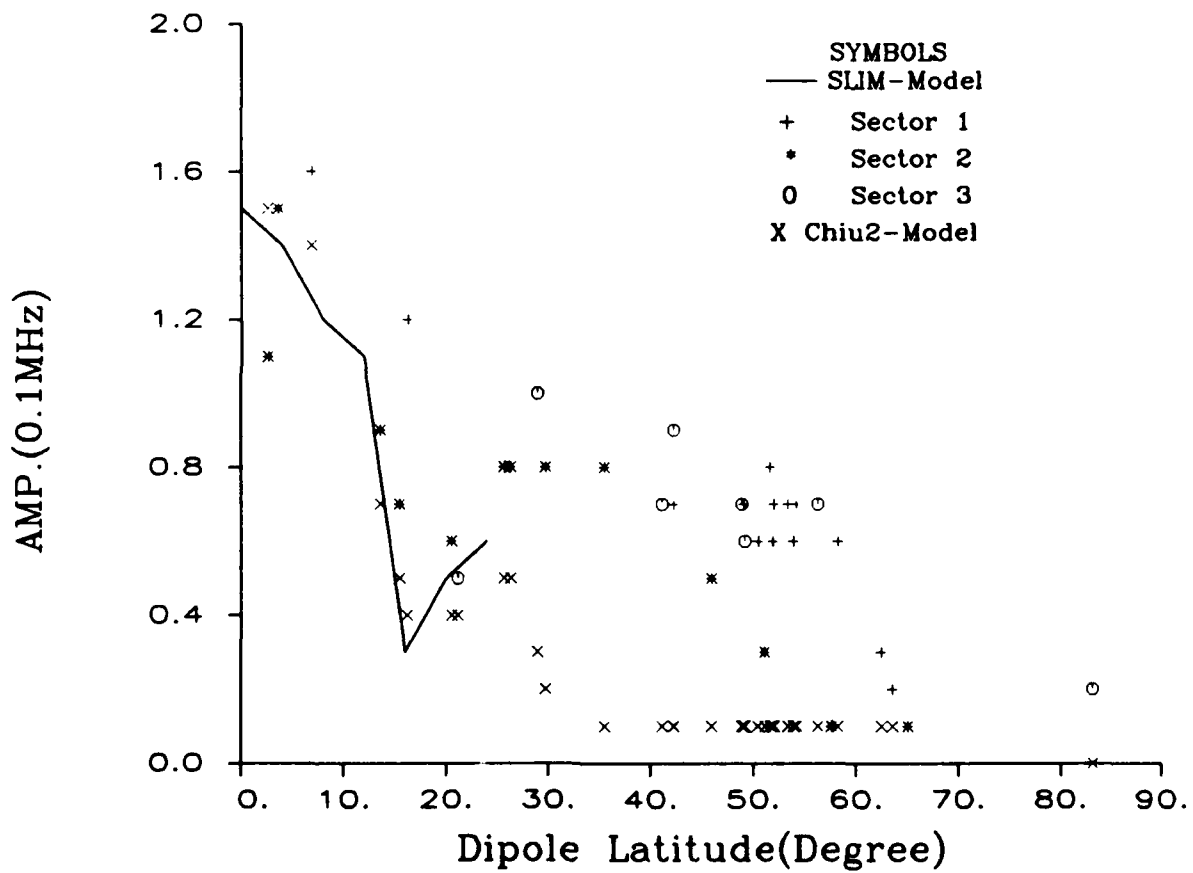


Figure B11. Same as B4, Except for foF2.

foF2

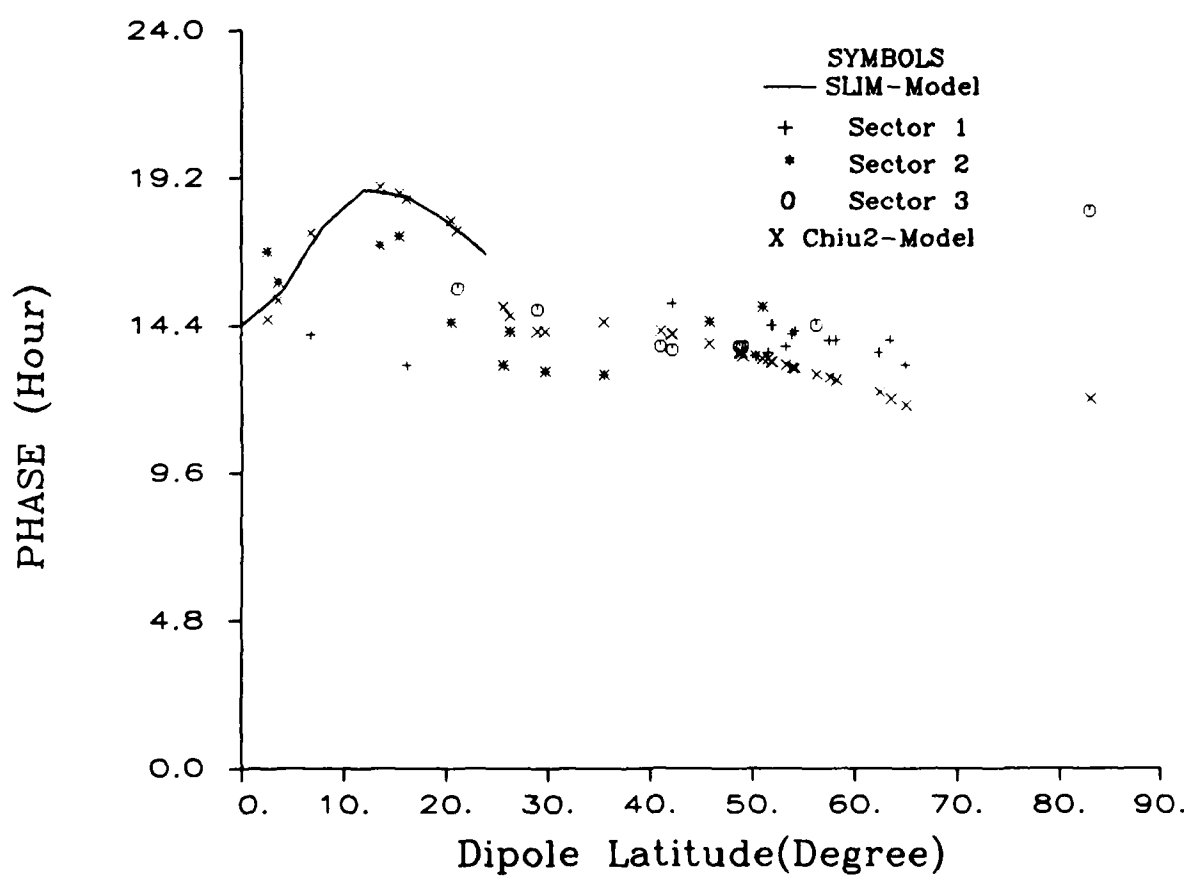


Figure B12. Same as B5, Except for foF2.

foF2

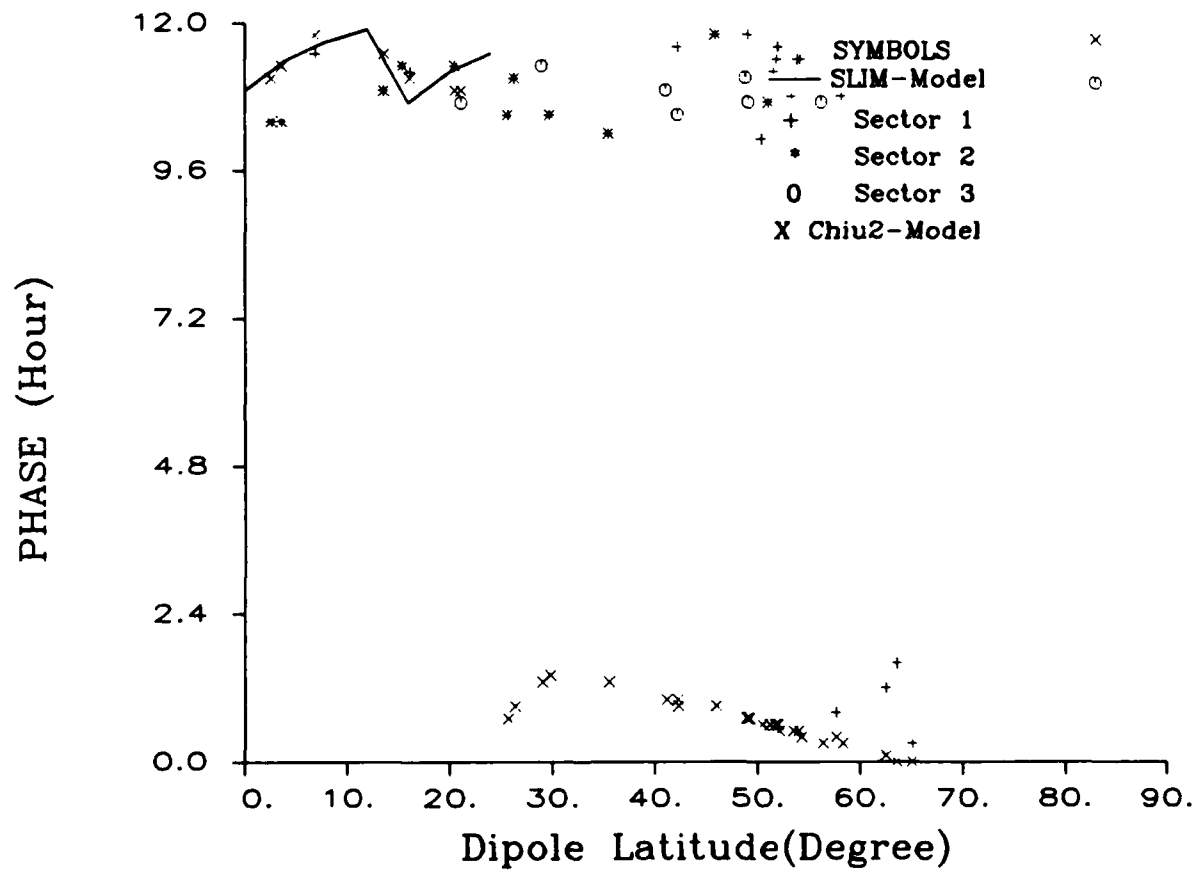


Figure B13. Same as B6, Except for foF2.

foF2

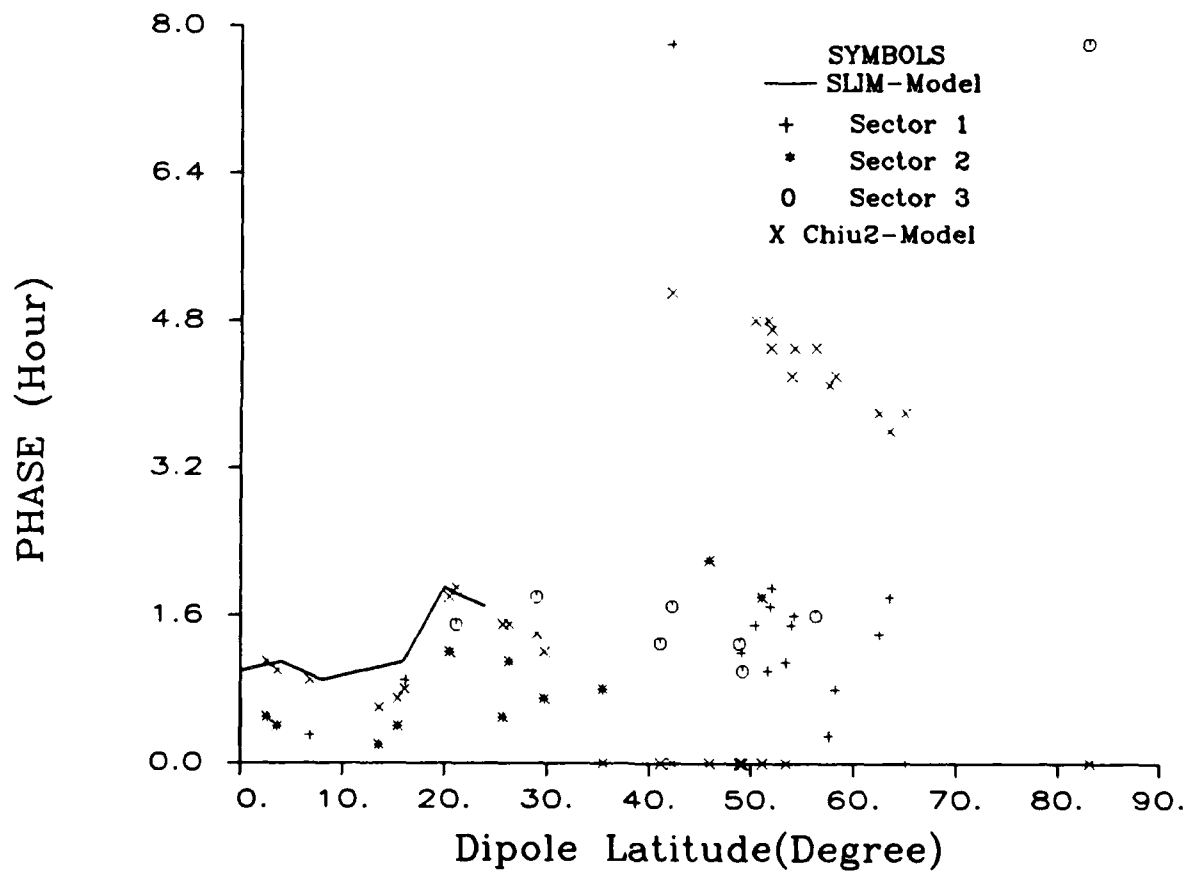


Figure B14. Same as B7, Except for foF2.